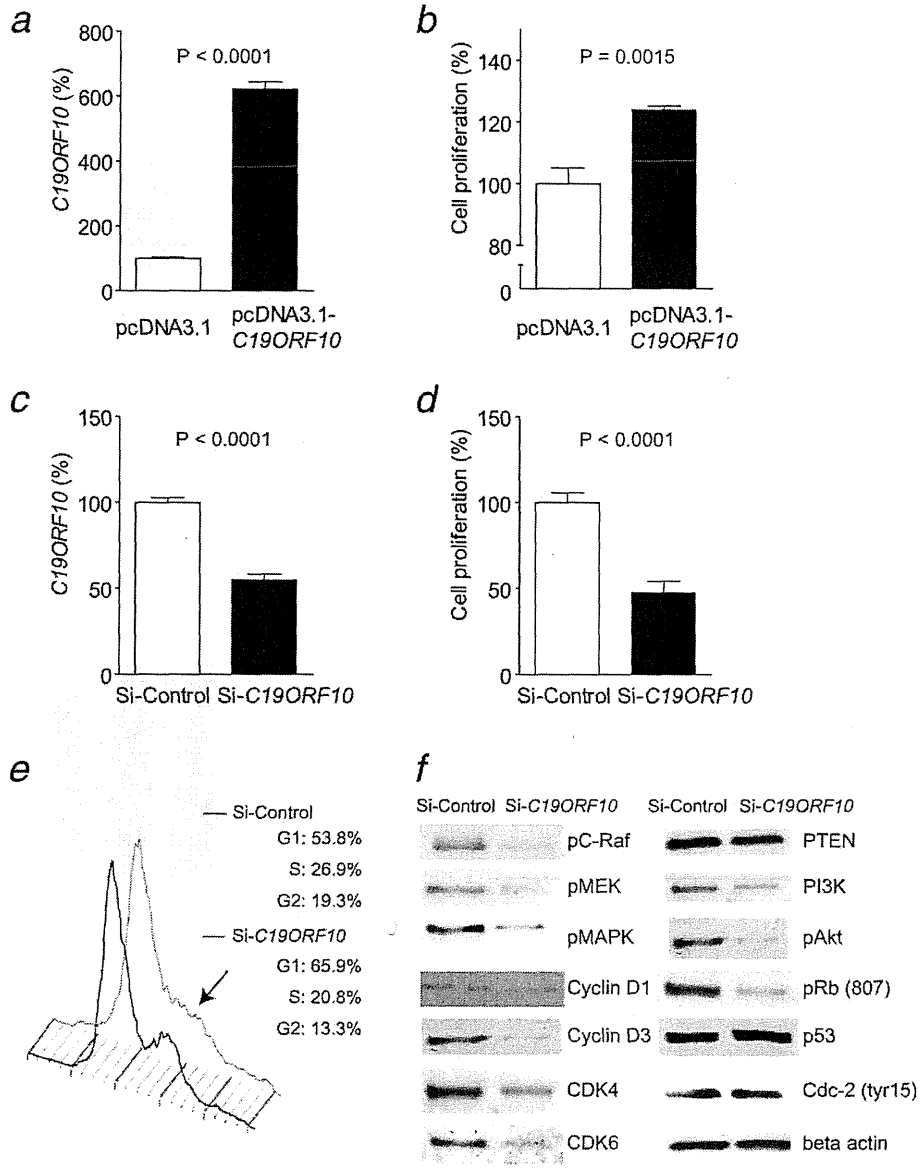

Figure 3. (*a*) RTD-PCR analysis of *c19orf10* expression in HLE cells transfected with pcDNA3.1 or pcDNA3.1-*c19orf10* plasmids. (*b*) Cell proliferation assay of HLE cells transfected with pcDNA3.1 or pcDNA3.1-*c19orf10* plasmids. Cell proliferation was evaluated 72 hr after each plasmid transfection. (*c*) RTD-PCR analysis of *c19orf10* expression in Hep3B cells transfected with Si-*Control* or Si-*c19orf10*. Gene expression was measured in triplicates 48 hr after transfection. (*d*) Cell proliferation assay of Hep3B cells transfected with Si-*Control* or Si-*c19orf10*. Cell proliferation was evaluated 72 hr after siRNA transfection. (*e*) Cell cycle analysis of HuH7 cells transfected with Si-*Control* or Si-*c19orf10*. Cell cycle was evaluated 72 hr after siRNA transfection. A black arrow indicates the G2 phase peak. (*f*) Western blotting analysis of Huh7 cells transfected with Si-*Control* or Si-*c19orf10*. Cells were lysed by RIPA buffer 72 hr after siRNA transfection.

pcDNA3.1 or pcDNA3.1-*c19orf10* plasmids, we identified an approximately sixfold overexpression of *c19orf10* when compared to the control 48 hr after transfection ($p < 0.0001$) (Fig. 3*a*). Interestingly, cell proliferation was modestly, but significantly, enhanced compared to the control 72 hr after transfection ($p = 0.0015$) (Fig. 3*b*).

We also transfected siRNAs targeting an irrelevant sequence (Si-*Control*) or *c19orf10* (Si-*c19orf10*) in Hep3B and

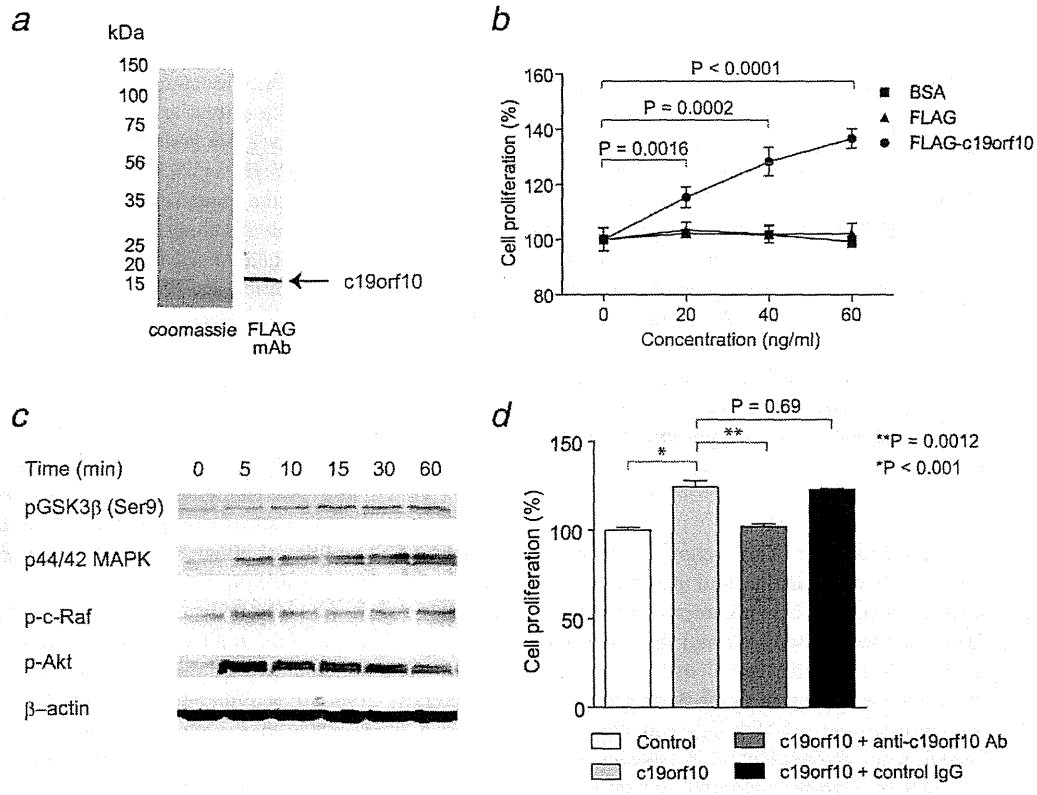

Figure 4. (*a*) Coomassie blue staining and Western blotting of culture supernatant of NIH3T3 cells transfected with pSI-*c19orf10-FLAG*. A black arrow indicates the 17-kDa c19orf10 protein. (*b*) Cell proliferation assay of HLE cells supplemented with recombinant c19orf10-FLAG, FLAG peptides or BSA. Cell proliferation was measured in quadruplicates 72 hr after supplementation. (*c*) Western blotting of HLE cells supplemented with c19orf10-FLAG (40 ng/ml). Cells were lysed at indicated time after c19orf10 supplementation. (*d*) Cell proliferation assay of HLE cells supplemented with control BSA (40 ng/ml) (white bar), c19orf10-FLAG (40 ng/ml) (light gray bar), c19orf10-FLAG (40 ng/ml) + anti-c19orf10 antibodies (gray bar) and c19orf10-FLAG (40 ng/ml) + control mouse IgG (black bar).

HuH7 cells. We observed an ~50% decrease in *c19orf10* expression in Hep3B cells transfected with Si- *c19orf10* compared to the control 48 hr after transfection with statistical significance ($p < 0.0001$). In this condition, cell proliferation was suppressed to 50% compared to the control 72 hr after transfection ($p < 0.0001$) (Figs. 3*c* and 3*d*). When we performed cell cycle analysis of HuH7 cells transfected with Si-*Control* or Si-*c19orf10*, we identified an increase of G1-phase cells and a decrease of S- and G2-phase cells by *c19orf10* knockdown, suggesting that the G1 cycle arrest was caused by the knockdown of *c19orf10* (Fig. 3*e*).

We examined the representative MAPK/Akt pathway-associated proteins and cell cycle regulators using Western blotting 72 hr after siRNAs transfection (Fig. 3*f*). Interestingly, phosphorylation of c-Raf, MEK, MAPK, PI3K and pAkt was inhibited by knockdown of *c19orf10*, suggesting the involvement of *c19orf10* in the MAPK/Akt pathways. Furthermore, phosphorylation of Rb, CDK4 and CDK6 was also inhibited by knockdown of *c19orf10*, consistent with the observation of G1 cell cycle arrest by *C19ORF10* knockdown. PTEN, p53 and phosphorylated CDC2 protein expression was not affected by knockdown of *c19orf10*.

C19orf10 encodes the secretory protein and stimulates cell proliferation

As the sequence of *c19orf10* suggested that it encodes a secretory protein, we transfected pSI-*c19orf10-FLAG* in NIH3T3 cells and examined the culture supernatant. Immunoprecipitation of the collected culture supernatant 48 hr after transfection using anti-FLAG antibodies indicated the existence of a 17-kDa protein (c19orf10), compatible with the molecular weight of the 142 amino acids protein encoded by *c19orf10* (Fig. 4*a*). We purified c19orf10-FLAG protein from the supernatant of HEK293 cells infected with Ad. *c19orf10-FLAG* using an anti-FLAG column. Supplementation of purified c19orf10-FLAG into the culture media for 72 hr enhanced the proliferation of HLE cells in a dose-dependent manner with statistical significance, whereas control FLAG peptides

and BSA had no effects on cell proliferation (Fig. 4*b*). Western blot analysis of HLE cells cultured with purified c19orf10-FLAG (40 ng/ml) or BSA control (40 ng/ml) indicated the immediate strong phospholyration of Akt peaked 5 min after supplementation (Fig. 4*c*). The modest phospholyration of GSK3β (Ser9) and p44/42 MAPK also followed and peaked 60 min after c19orf10 supplementation. These data suggest that Akt pathway might be directly involved in the c19orf10-mediated cell proliferation signaling with the subsequent activation of MAPK pathway. Furthermore, addition of antibodies against c19orf10 to the culture media abolished the cell proliferation induced by c19orf10, whereas control IgG had no effects (Fig. 4*d*). Taken together, these data suggest that c19orf10 may be a growth factor overexpressed in AFP-positive HCCs and activates the Akt/MAPK pathways, potentially through the activation of an unidentified c19orf10 receptor.

Discussion

SAGE facilitates the measurement of transcripts from normal and malignant tissues in a nonbiased and highly accurate, quantitative manner. Indeed, SAGE produces a comprehensive gene expression profile without *a priori* gene sequence information, leading to the identification of novel transcripts potentially involved in the pathogenesis of human cancer.[19] In our study, we identified seven SAGE tags potentially corresponding to novel genes activated in HCC. Among them, we identified the secretory protein c19orf10 activated in a subset of HCCs.

Several serum markers including AFP, DCP and Glypican 3 are currently used for the detection and/or the evaluation of the treatment for HCCs in the clinic.[15–18,35] These markers are known as oncofetal proteins, that is, expressed in the fetus, transcriptionally suppressed in the adult organ and reactivated in the tumor. We identified that the expression of *c19orf10* positively correlated with *AFP* expression but did not correlate with the expression of *GPC3* or the biliary marker *KRT19*. As *c19orf10* was rarely detected in the normal liver, it is possible that c19orf10 is also an oncofetal protein activated in HCC. We are currently developing a system to detect serum c19orf10 in HCC patients, and the significance of the serum c19orf10 value as an HCC marker should be clarified.

Recent advancement in molecular biology has revealed the considerable diversity of transcription initiation and/or termination of genes altered in the process of carcinogenesis. Indeed, using 5′ SAGE approach, we recently discovered the novel intronic transcripts activated in HCC.[36] Interestingly, when we investigated the transcription initiation of *c19orf10* using the 5′ SAGE database, we identified a potential 5′ splice variant initiated from the second exon of *c19orf10* (data not shown). Although we have not yet validated the presence of 5′ splice variants in *c19orf10* by PCR, examination of 5′ EST database also suggested the presence of the similar splice variants (GenBank Accession Number CR980295, BQ680744, BQ648461, *etc.*). Alteration of transcription initiation/termination in *c19orf10* might affect the abundance or function of c19orf10 protein, and the details of 5′ splice variants in *c19orf10* should be clarified in future studies.

Molecular targeting therapy has rapidly emerged for solid tumors as well as for leukemia.[37–39] Sorafenib is a multikinase inhibitor targeting Raf kinase in the MAPK pathway as well as VEGFR and the platelet-derived growth factor receptor.[40,41] In our study, we identified that c19orf10 activates the MAPK and Akt/PI3K pathways and contributes to the proliferation of HCC cell lines, although we still could not discover the potential receptor of c19orf10. Development of a neutralizing c19orf10 antibody may provide novel therapeutic options for HCC patients to inhibit these signaling pathways, and its efficacy should be evaluated in the future.

Recently, c19orf10 was found to be expressed in fibroblast-like synoviocytes in the synovium using a proteomics approach.[29] In addition, a recent article indicated that c19orf10 was expressed in preadipocyte cells and involved in adipogenesis using two-dimensional electrophoresis mass spectrometry analysis.[28] Thus, c19orf10 may have pleiotropic effects on various lineages of normal organs in various developmental stages, and the clarification of its distribution and biological properties in the whole body may provide more detailed information about the function of c19orf10.

In conclusion, we have identified the protein c19orf10 that regulates the Akt/MAPK pathways and cell cycle through an unidentified mechanism in HCC. Although further studies should be conducted to detect the potential c19orf10 receptor or signaling molecules binding to c19orf10, our study suggests that c19orf10 may be a novel growth factor, a potential tumor marker and also a potential target molecule for HCC treatment.

Acknowledgements

The authors thank Ms. Mikie Kakiuchi, Ms. Masayo Baba and Ms. Nami Nishiyama for their excellent technical assistance.

References

1. Befeler AS, Di Bisceglie AM. Hepatocellular carcinoma: diagnosis and treatment. *Gastroenterology* 2002;122: 1609–19.
2. Tsukuma H, Hiyama T, Tanaka S, Nakao M, Yabuuchi T, Kitamura T, Nakanishi K, Fujimoto I, Inoue A, Yamazaki H, Kawashima T. Risk factors for hepatocellular carcinoma among patients with chronic liver disease. *N Engl J Med* 1993;328:1797–801.
3. Liang TJ, Jeffers LJ, Reddy KR, De Medina M, Parker IT, Cheinquer H, Idrovo V, Rabassa A, Schiff ER. Viral pathogenesis of hepatocellular carcinoma in the United States. *Hepatology* 1993;18:1326–33.
4. Mayans MV, Calvet X, Bruix J, Bruguera M, Costa J, Esteve J, Bosch FX, Bru C, Rodes J. Risk factors for hepatocellular carcinoma in Catalonia, Spain. *Int J Cancer* 1990;46:378–81.

5. Mohamed AE, Kew MC, Groeneveld HT. Alcohol consumption as a risk factor for hepatocellular carcinoma in urban southern African blacks. *Int J Cancer* 1992; 51:537–41.
6. Smedile A, Bugianesi E. Steatosis and hepatocellular carcinoma risk. *Eur Rev Med Pharmacol Sci* 2005;9:291–3.
7. Floreani A, Baragiotta A, Baldo V, Menegon T, Farinati F, Naccarato R. Hepatic and extrahepatic malignancies in primary biliary cirrhosis. *Hepatology* 1999; 29:1425–8.
8. Tradati F, Colombo M, Mannucci PM, Rumi MG, De Fazio C, Gamba G, Ciavarella N, Rocino A, Morfini M, Scaraggi A, Taioli E. A prospective multicenter study of hepatocellular carcinoma in italian hemophiliacs with chronic hepatitis C. The Study Group of the Association of Italian Hemophilia Centers. *Blood* 1998;91:1173–7.
9. Jones DE, Metcalf JV, Collier JD, Bassendine MF, James OF. Hepatocellular carcinoma in primary biliary cirrhosis and its impact on outcomes. *Hepatology* 1997; 26:1138–42.
10. Caballeria L, Pares A, Castells A, Gines A, Bru C, Rodes J. Hepatocellular carcinoma in primary biliary cirrhosis: similar incidence to that in hepatitis C virus-related cirrhosis. *Am J Gastroenterol* 2001; 96:1160–3.
11. Yoshida H, Shiratori Y, Moriyama M, Arakawa Y, Ide T, Sata M, Inoue O, Yano M, Tanaka M, Fujiyama S, Nishiguchi S, Kuroki T, et al. Interferon therapy reduces the risk for hepatocellular carcinoma: national surveillance program of cirrhotic and noncirrhotic patients with chronic hepatitis C in Japan. IHIT Study Group. Inhibition of Hepatocarcinogenesis by Interferon Therapy. *Ann Intern Med* 1999; 131:174–81.
12. Yuen MF, Cheng CC, Lauder IJ, Lam SK, Ooi CG, Lai CL. Early detection of hepatocellular carcinoma increases the chance of treatment: Hong Kong experience. *Hepatology* 2000;31:330–5.
13. Peterson MS, Baron RL. Radiologic diagnosis of hepatocellular carcinoma. *Clin Liver Dis* 2001;5:123–44.
14. Choi BI. The current status of imaging diagnosis of hepatocellular carcinoma. *Liver Transpl* 2004;10:S20–S25.
15. Fujiyama S, Tanaka M, Maeda S, Ashihara H, Hirata R, Tomita K. Tumor markers in early diagnosis, follow-up and management of patients with hepatocellular carcinoma. *Oncology* 2002;62 (Suppl 1):57–63.
16. Tsai SL, Huang GT, Yang PM, Sheu JC, Sung JL, Chen DS. Plasma des-gamma-carboxyprothrombin in the early stage of hepatocellular carcinoma. *Hepatology* 1990; 11:481–8.
17. Ikoma J, Kaito M, Ishihara T, Nakagawa N, Kamei A, Fujita N, Iwasa M, Tamaki S, Watanabe S, Adachi Y. Early diagnosis of hepatocellular carcinoma using a sensitive assay for serum des-gamma-carboxy prothrombin: a prospective study. *Hepatogastroenterology* 2002; 49:235–8.
18. Kasahara A, Hayashi N, Fusamoto H, Kawada Y, Imai Y, Yamamoto H, Hayashi E, Ogihara T, Kamada T. Clinical evaluation of plasma des-gamma-carboxy prothrombin as a marker protein of hepatocellular carcinoma in patients with tumors of various sizes. *Dig Dis Sci* 1993; 38:2170–6.
19. Yamashita T, Honda M, Kaneko S. Application of serial analysis of gene expression in cancer research. *Curr Pharm Biotechnol* 2008;9:375–82.
20. Cheng AL, Kang YK, Chen Z, Tsao CJ, Qin S, Kim JS, Luo R, Feng J, Ye S, Yang TS, Xu J, Sun Y, et al. Efficacy and safety of sorafenib in patients in the Asia-Pacific region with advanced hepatocellular carcinoma: a phase III randomised, double-blind, placebo-controlled trial. *Lancet Oncol* 2009;10:25–34.
21. Llovet JM, Ricci S, Mazzaferro V, Hilgard P, Gane E, Blanc JF, de Oliveira AC, Santoro A, Raoul JL, Forner A, Schwartz M, Porta C, et al. Sorafenib in advanced hepatocellular carcinoma. *N Engl J Med* 2008;359:378–90.
22. Yamashita T, Hashimoto S, Kaneko S, Nagai S, Toyoda N, Suzuki T, Kobayashi K, Matsushima K. Comprehensive gene expression profile of a normal human liver. *Biochem Biophys Res Commun* 2000;269: 110–16.
23. Yamashita T, Honda M, Takatori H, Nishino R, Hoshino N, Kaneko S. Genome-wide transcriptome mapping analysis identifies organ-specific gene expression patterns along human chromosomes. *Genomics* 2004;84:867–75.
24. Yamashita T, Honda M, Takatori H, Nishino R, Minato H, Takamura H, Ohta T, Kaneko S. Activation of lipogenic pathway correlates with cell proliferation and poor prognosis in hepatocellular carcinoma. *J Hepatol* 2009;50:100–10.
25. Yamashita T, Kaneko S, Hashimoto S, Sato T, Nagai S, Toyoda N, Suzuki T, Kobayashi K, Matsushima K. Serial analysis of gene expression in chronic hepatitis C and hepatocellular carcinoma. *Biochem Biophys Res Commun* 2001;282:647–54.
26. Tulin EE, Onoda N, Nakata Y, Maeda M, Hasegawa M, Nomura H, Kitamura T. SF20/IL-25, a novel bone marrow stroma-derived growth factor that binds to mouse thymic shared antigen-1 and supports lymphoid cell proliferation. *J Immunol* 2001;167:6338–47.
27. Tulin EE, Onoda N, Nakata Y, Maeda M, Hasegawa M, Nomura H, Kitamura T. SF20/IL-25, a novel bone marrow stroma-derived growth factor that binds to mouse thymic shared antigen-1 and supports lymphoid cell proliferation. *J Immunol* 2003;170:1593.
28. Wang P, Mariman E, Keijer J, Bouwman F, Noben JP, Robben J, Renes J. Profiling of the secreted proteins during 3T3-L1 adipocyte differentiation leads to the identification of novel adipokines. *Cell Mol Life Sci* 2004;61:2405–17.
29. Weiler T, Du Q, Krokhin O, Ens W, Standing K, El-Gabalawy H, Wilkins JA. The identification and characterization of a novel protein, c19orf10, in the synovium. *Arthritis Res Ther* 2007;9:R30.
30. Takatori H, Yamashita T, Honda M, Nishino R, Arai K, Takamura H, Ohta T, Zen Y, Kaneko S. dUTP pyrophosphatase expression correlates with a poor prognosis in hepatocellular carcinoma. *Liver Int* 2010; 30:438–46.
31. Sakai Y, Honda M, Fujinaga H, Tatsumi I, Mizukoshi E, Nakamoto Y, Kaneko S. Common transcriptional signature of tumor-infiltrating mononuclear inflammatory cells and peripheral blood mononuclear cells in hepatocellular carcinoma patients. *Cancer Res* 2008;68: 10267–79.
32. Honda M, Yamashita T, Ueda T, Takatori H, Nishino R, Kaneko S. Different signaling pathways in the livers of patients with chronic hepatitis B or chronic hepatitis C. *Hepatology* 2006;44:1122–38.
33. Sakai Y, Morrison BJ, Burke JD, Park JM, Terabe M, Janik JE, Forni G, Berzofsky JA, Morris JC. Vaccination by genetically modified dendritic cells expressing a truncated neu oncogene prevents development of breast cancer in transgenic mice. *Cancer Res* 2004;64:8022–8.
34. Sakai Y, Kaneko S, Nakamoto Y, Kagaya T, Mukaida N, Kobayashi K. Enhanced anti-tumor effects of herpes simplex virus thymidine kinase/ganciclovir system by codelivering monocyte chemoattractant protein-1 in hepatocellular carcinoma. *Cancer Gene Ther* 2001;8:695–704.
35. Capurro M, Wanless IR, Sherman M, Deboer G, Shi W, Miyoshi E, Filmus J. Glypican-3: a novel serum and histochemical marker for hepatocellular carcinoma. *Gastroenterology* 2003;125: 89–97.
36. Hodo Y, Hashimoto S, Honda M, Yamashita T, Suzuki Y, Sugano S, Kaneko S, Matsushima K. Comprehensive gene expression analysis of 5′-end of mRNA identified novel intronic transcripts associated with hepatocellular carcinoma. *Genomics* 2010;95:217–23.

37. Romond EH, Perez EA, Bryant J, Suman VJ, Geyer CE, Jr, Davidson NE, Tan-Chiu E, Martino S, Paik S, Kaufman PA, Swain SM, Pisansky TM, et al. Trastuzumab plus adjuvant chemotherapy for operable HER2-positive breast cancer. *N Engl J Med* 2005;353:1673–84.
38. Hurwitz H, Fehrenbacher L, Novotny W, Cartwright T, Hainsworth J, Heim W, Berlin J, Baron A, Griffing S, Holmgren E, Ferrara N, Fyfe G, et al. Bevacizumab plus irinotecan, fluorouracil, and leucovorin for metastatic colorectal cancer. *N Engl J Med* 2004;350:2335–42.
39. Shepherd FA, Rodrigues Pereira J, Ciuleanu T, Tan EH, Hirsh V, Thongprasert S, Campos D, Maoleekoonpiroj S, Smylie M, Martins R, van Kooten M, Dediu M, et al. Erlotinib in previously treated non-small-cell lung cancer. *N Engl J Med* 2005; 353:123–32.
40. Llovet JM, Bruix J. Molecular targeted therapies in hepatocellular carcinoma. *Hepatology* 2008;48:1312–27.
41. Liu L, Cao Y, Chen C, Zhang X, McNabola A, Wilkie D, Wilhelm S, Lynch M, Carter C. Sorafenib blocks the RAF/MEK/ERK pathway, inhibits tumor angiogenesis, and induces tumor cell apoptosis in hepatocellular carcinoma model PLC/PRF/5. *Cancer Res* 2006;66: 11851–8.

Biochemical and Biophysical Research Communications 400 (2010) 461–465

Contents lists available at ScienceDirect

Biochemical and Biophysical Research Communications

journal homepage: www.elsevier.com/locate/ybbrc

Efficiently differentiating vascular endothelial cells from adipose tissue-derived mesenchymal stem cells in serum-free culture

Masamitsu Konno [a,b], Tatsuo S. Hamazaki [a,*], Satsuki Fukuda [a], Makoto Tokuhara [a], Hideho Uchiyama [c], Hitoshi Okazawa [b], Hitoshi Okochi [a,1], Makoto Asashima [d,1]

[a] Department of Regenerative Medicine, Research Institute, National Center for Global Health and Medicine, Tokyo 162-8655, Japan
[b] Department of Neuropathology, Medical Research Institute, Tokyo Medical and Dental University, Tokyo 113-8510, Japan
[c] International Graduate School of Arts and Science, Yokohama City University, Yokohama 236-0027, Japan
[d] Department of Life Sciences (Biology), Graduate School of Arts and Sciences, The University of Tokyo, Tokyo 153-8902, Japan

ARTICLE INFO

Article history:
Received 27 July 2010
Available online 12 August 2010

Keywords:
Adipose-derived mesenchymal stem cell
Vascular endothelial cell
Differentiation
Serum-free culture
FGF2

ABSTRACT

Adipose tissue-derived mesenchymal stem cells (ASCs) have been reported to be multipotent and to differentiate into various cell types, including osteocytes, adipocytes, chondrocytes, and neural cells. Recently, many authors have reported that ASCs are also able to differentiate into vascular endothelial cells (VECs) in vitro. However, these reports included the use of medium containing fetal bovine serum for endothelial differentiation. In the present study, we have developed a novel method for differentiating mouse ASCs into VECs under serum-free conditions. After the differentiation culture, over 80% of the cells expressed vascular endothelial-specific marker proteins and could take up low-density lipoprotein in vitro. This protocol should be helpful in clarifying the mechanisms of ASC differentiation into the VSC lineage.

1. Introduction

Recently, adipose tissue is an important source of adult stem cells [1]. Adipose-derived mesenchymal stem cells (ASCs) can be obtained in high yield with minimal discomfort under local anesthesia [2,3]. After the reports of Zuk et al. [4,5], many studies have examined the plasticity, induction ability, and individual characteristics of ASCs. Derived from the embryonic mesoderm, adipose tissue is a heterogeneous cell population that includes smooth muscle cells, fibroblasts, adipocytes, mast cells, and endothelial cells [6–8]. ASCs are an adherent cell population in vitro and maintain their mesenchymal phenotype and plasticity towards the mesenchymal lineage even after they propagate in culture for several passages. These cells can differentiate into several cell types in vitro, including adipocytes, chondrocytes, osteoblasts, cardiomyocytes, and endothelial cells [5,9–13]. Moreover, ASCs are reported to have positive effects on patients who received bone marrow transplantation and suffered from GVHD (graft versus host disease), suggesting that they have an immuno-modulatory function [14].

In the present study, we focused on whether ASCs are able to differentiate into vascular endothelial cells (VECs) in a chemically defined medium after expanding them. Although mouse [15], rat [16], and human [13,17–19] ASCs have already been reported to differentiate into VECs, all of the differentiation methods have utilized fetal bovine serum (FBS). When considering the clinical applications for regenerative medicine in the future, possible contamination by animal serum is a negative factor for safety. Unknown factors in FBS also prevent researchers from accurate analysis of the differentiation mechanism. Therefore, we attempted to develop a new method for differentiating ASCs into functional VECs without serum.

2. Materials and methods

2.1. Isolation of ASCs from mice

Inguinal adipose tissue was isolated from 12- to 14-week-old adult female and GFP-transgenic C57BL/6J mice. The tissue was minced into 2–3 mm pieces in DMEM (Gibco) containing 10% FBS, and incubated at 37 °C in 5% CO_2 incubator for 1 h. Then the suspension was centrifuged at 1300 rpm for 6 min at room temperature. To dissociate the cells, they were treated with 0.12% collagenase type I solution and incubated at 37 °C for 30 min and then centrifuged at 1300 rpm for 6 min at room temperature. The cells were cultured in DMEM containing 5% FBS, 10 units penicillin,

* Corresponding author. Address: Department of Regenerative Medicine, Research Institute, National Center for Global Health and Medicine, Toyama 1-21-1, Shinjuku, Tokyo 162-8655, Japan. Fax: +81 3 3202 7192.
E-mail address: hamazaki@ri.ncgm.go.jp (T.S. Hamazaki).
[1] These authors contributed equally to this work.

0006-291X/$ - see front matter © 2010 Elsevier Inc. All rights reserved.
doi:10.1016/j.bbrc.2010.08.029

and 10 μg/ml streptomycin (GIBCO) in a CO_2 incubator at 37 °C. After continuous culture for five passages, they were used for the differentiation experiments. To eliminate any intact VECs, CD31 positive cells were removed using anti-CD31 antibody-conjugated beads (MACS) after 2 h incubation of the preparation. The CD31 negative cells were cultured and serially passaged. Animal experiments were approved by the Animal Care and Use Committee of National Center for Global Health and Medicine.

2.2. Examination of ASCs differentiation capacity into adipogenic and osteogenic differentiation

To confirm the multipotency of our cultured ASCs, we tested whether they could differentiate into adipocytes and osteoblasts, as reported previously. Passage 5 cells were cultured in adipogenic medium for 2 weeks; hMSC Adipogenic Induction SingleQuots (Cambrex) supplemented with indometacin, IBMX, insulin, dexamethasone, NCGS, and L-glutamine. The cells were fixed in 10% formalin for 10 min and stained with Oil red-O solution (Merck) to detect lipid droplets. To confirm osteogenic differentiation, the cells were cultured in osteogenic medium: hMSC Osteogenic SingleQuots (Cambrex) supplemented with ascorbate, MCGS, β-glycerophosphate, and L-glutamine. After 2 weeks, the alkaline phosphatase activity of the cells was measured by Alkaline Phosphatase Kit (Takara Bio) and the expression of an osteogenic protein marker, osteopontin, was examined by reverse transcriptase-polymerase chain reaction (RT-PCR).

2.3. Differentiation into vascular endothelial cells

To initially determine whether the ASCs could develop the characteristics of VECs or not, they were cultured in a commercially available vascular cell maintaining medium, EBM-2 (CAMBREX) containing 2% FBS and EGM-2 BulletKit (mixture of FGF2, VEGF, heparin, IGF-I, EGF, hydrocortisone, and ascorbic acid, CAMBREX) on collagen type IV coated dish, for 12 days; then their gene expression was verified. Next, we surveyed supplements that are able to replace FBS. We tested 2% KSR, B27, N2, G5, or ITS (Invitrogen); each candidate supplement was added in EBM-2 medium instead of FBS. And we also examined the other culture medium such as DMEM, IMDM, and DMEM/F12 instead of EBM-2. Finally, to determine the optimal concentration of FGF2 or VGEF, different concentrations (0, 5, 10, and 20 ng/ml) was tested for induction of endothelial cells. When the optimal culture medium for the VEC induction from ASCs was determined to be DMEM/F12 medium containing 10 ng/ml FGF2, 2% ITS, and EGM-2 BulletKit (without FGF2), further experiments for functional assay and transplantation employed this medium.

2.4. RT-PCR and real time PCR

Marker gene expression of VECs was determined by RT-PCR. After ASCs were cultured for 12 days in endothelial differentiation medium on a collagen type IV dish, total RNA was extracted by the use of Isogen (Nippon gene) as described by the manufacturer, and was treated with Superscript III (Invitrogen) to generate cDNA using oligo(dT) adaptor primer (Sigma). Then PCR amplification was performed for mouse *flk1*, *flt1*, *VE-cadherin*, and *CD31*. PCR cycles were as follows: 95 °C for 5 min, 95 °C for 30 s, annealing temperature for 30 s, 72 °C for 1 min (25–30 cycles), and 72 °C for 3 min. The RT-PCR products ware analyzed by 1% agarose gel electrophoresis and visualized with ethidium bromide. Primers for PCR were follows: *flk1* (5′-GCC AAT GAAGGG GAACTGAAGAC-3′, 5′-TCTGGCT GCTGGTGATGCTGTC-3′), *flt1* (5′-TGTGGAGAAACTTGGTGACCT-3′, 5′-TGGAGAACAGCAGGACTCCTT-3′), *ve-cadherin* (5′-TTGCCCAGCCC TACGAACCTAAAG-3′, 5′-ACCACCGCCCTCCTCATCGTAAGT-3′), *CD31* (5′-GGTGACACTGGACAAAAAGG-3′, 5′-CAGCTTCACTGCTTTGCTT G-3′), *gapdh* (5′-TGAAGGTCGGTGTGAACGGATTTGGC-3′, 5′-CATG TAGGCCATGAGGTCCACCAC-3′). For the real-time PCR, primers are follows: *tie2* (5′-GTGAAGATCAAGAATGCTACC-3′, 5′-GTGAAGATC AAGAATGCTACC-3′), *CD31* (5′-GTTTGTCAAGCGAAGGATAGATA A-3′, 5′-TCCTGCACGGTGACGTATTCACT-3′), *von Willebrand factor* (*vWF*, 5′-AACGGAAGTCCATGGTTCTG-3′, 5′-CCCCATTGAAGGCAT ACTCC-3′). Reactions were performed using SYBER Premix ExTaq (Takara Bio) and a MyiQ thermal cycler (BIORAD).

2.5. Immunocytochemistry

Differentiated endothelial-like cells from ASCs were fixed with 4% paraformaldehyde for 30 min at room temperature and then treated successively with 0.3% Triton X-100 (Wako Chemical) in PBS (Sigma) for 15 min followed by 3% bovine serum albumin (Sigma) for 30 min to reduce nonspecific reactions. The cells were reacted overnight with each of the following anti-endothelial marker antibodies at a 1:300 dilution at 4 °C; anti-flk1 (Becton Dickinson), anti-CD34 (Becton Dickinson), and anti-tie2 (Santa Cruz Biotechnology) antibodies. Then the cells were stained by Alexa Fluor 488 or 594 conjugated antibody (Molecular Probes) as the secondary antibody for 1 h at room temperature. Their nuclei were stained with DAPI for 10 min. The photographs were taken with a DP70 digital camera (Olympus) and analyzed by MetaMorph software (Molecular Devices).

2.6. Examination of cell function in vivo and in vitro

For the examination of tubular formation, the cells were seeded on Matrigel (Becton Dickinson) at 5×10^4 cells/35 mm dish. After 24 h, the morphology of the cells was examined, and phase-contrast images were photographed (Olympus IX70). For in vivo examination, the femoral muscle of a mouse was injured by liquid nitrogen and injected with the differentiated vascular endothelial-like cells (1×10^6 cells) from ASCs of GFP-transgenic mice. Two weeks after cell injection, we investigated whether the donor cells had formed vessel-like structures.

LDL uptake was assessed by incubating cells for 4 h at 37 °C with 2.5 μg/ml Alexa Fluor 488 conjugated acetyl-LDL (Molecular Probes). Cells were analyzed by fluorescence microscopy and a flow cytometer (EPICS XL, Beckman Coulter).

3. Results

3.1. In vitro differentiation of ASCs

To prove that the cultured cells from adipose tissue had retained their multipotent differentiation potential, we first confirmed that they differentiated into adipogenic and osteogenic lineages. When ASCs (Fig. 1A) were cultured in adipogenic medium for 2 weeks, more than 40% of the cells became lipid-retaining cells that stained by Oil-red O (Fig. 1B). In osteogenic medium, more than 50% of the cells were induced into an osteogenic lineage confirmed by alkaline phosphatase staining (Fig. 1C). The gene expression of *osteopontin* was also detected (Fig. 1D).

3.2. ASCs cultured in growth factor mix changed their gene expression pattern to closely resemble that of vascular endothelial cells

It was reported that the early passages of ASCs can contain small amounts of VECs and express VEC marker proteins [20]. Therefore, we used anti-CD31 antibody to remove any CD31 positive cells during the preparation of ASCs. To examine whether the ASCs could differentiate into VECs in "vascular endothelial maintaining

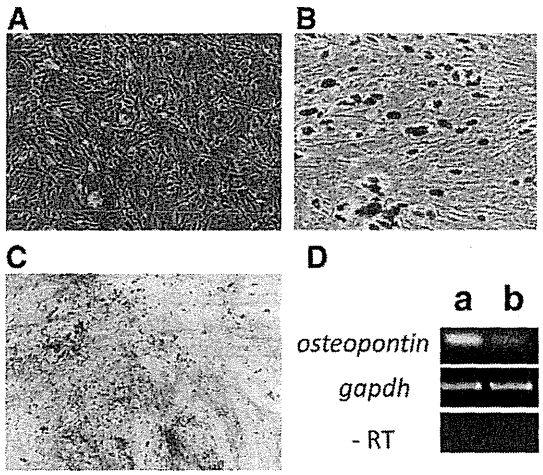

Fig. 1. Examination of mouse adipose-derived mesenchymal stem cell (ASCs) differentiation capacity into adipogenic and osteogenic lineages. (A) Mouse ASCs after five passages. (B) ASCs were cultured in adipogenic medium for 2 weeks. About 40% of the cells were stained by Oil-red O, indicating they differentiated into mature adipocytes. (C) More than 50% of the cells were positive for alkaline phosphatase staining after 2 weeks cultured in osteogenic medium, and they also express an osteopontin gene. (D) a: cultured in the osteogenic medium, b: cultured in normal ASCs medium.

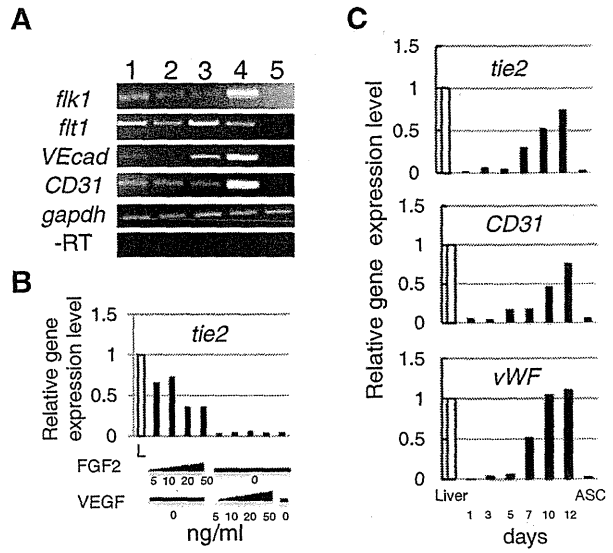

Fig. 2. Vascular endothelial-specific gene expression analyzes in different culture media. (A) RT-PCR analysis of ASCs cultured in EBM-2 medium containing EGM-2 BulletKit in the presence of FBS for 12 days (lane 1). ASCs cultured in EBM-2 containing EGM-2 BulletKit and ITS (lane 2). ASCs cultured in DMEM/F12 medium containing EGM-2 BulletKit and ITS (lane 3). Compared to the "vascular endothelial maintained medium" containing FBS (lane 1), *ve-cadherin* expression was observed almost the same level when ASCs cultured in serum-free DMEM/F12 medium (lane 3). For comparison, 8-week-old mouse liver cells (lane 4) and normal ASCs (lane 5) are shown. (B) Effects of FGF2 and VEGF in different concentrations on the differentiation of ASCs Expression of *tie2*, one of the vascular endothelial markers, was highest when 10 ng/ml FGF2 containing medium was used. *Tie2* gene expression did not elevate in any concentrations of VEGF in the absence of FGF2 and serum L (liver used as positive control). (C) Time course expression of *tie2*, *CD31*, and *vWF* genes. All of genes were upregulated 7–10 days after the beginning of differentiation culture. ASCs were differentiated in DMEM/F12 medium containing EGM-2 BulletKit (without FGF2), ITS, and 10 ng/ml FGF-2.

medium", we cultured ASCs in EBM-2 medium containing 2% FBS and EGM-2 BulletKit on a collagen type IV coated dish. After 12 days of culture, they expressed the vascular endothelial marker genes, *flk1*, *flt1*, *ve-cadherin*, and *CD31* (Fig. 2A, lane 1). Normal ASCs did not express these genes at all (Fig. 2A, lane 5). These results indicate that the ASCs have capacity to differentiate into VECs. The "vascular endothelial maintaining medium" contains 2% FBS, which may contain variable amounts of unknown factors including growth factors. To establish a stable method for differentiating VECs from ASCs, we tried to establish a serum-free culture method. We tested 2% KSR, B27, N2, G5, and ITS as replacements for FBS and found that the ITS supplement (insulin, transferrin, and selenium) had almost the same effects as FBS on endothelial differentiation. The cells expressed *flk1*, *flt1* and *CD31* but did not express *ve-cadherin* (Fig. 2A, lane 2). Others supplements were not so much upregulated the gene expressions except for ITS (data not shown). Therefore, we tested other types of basal medium, DMEM, IMDM, and DMEM/F12, as replacements for EBM-2. When we changed the medium from EBM-2 to DMEM/F12, the gene expression of *ve-cadherin* was proven (Fig. 2A, lane 3). There was no effect was observed when the medium was used DMEM or IMDM (data not shown).

Next, we attempted to determine the optimal concentrations of FGF2 and VEGF, because both factors are considered to be important for the differentiation of VECs [21,22]. The ASCs were seeded in DMEM/F12 medium containing ITS and EGM-2 Bulletkit (without FGF2 and VEGF). Then we added various concentrations of FGF2 or VEGF to the culture medium. After 12 days, we analyzed for expression of the early vascular endothelial marker gene, *tie2*, by real-time PCR. Without FGF2, expressions of vascular endothelial marker genes did not increase (Fig. 2B) even when the concentration of VEGF was elevated. On the other hand, in the presence of FGF2, *tie2* expression level increased, and 10 ng/ml FGF2 was the most efficient concentration (Fig. 2B). These results indicate that, when the ASCs differentiate into VECs in this serum-free medium, FGF2 plays a more important role than VEGF.

When we examined the time course expression of vascular endothelium-specific genes of ASCs cultured in this differentiation medium, *tie2* and *CD31* showed almost the same pattern of expression, beginning to express after 5–7 days culture and increasing gradually up to 12 days. Gene expression of *vWF* increased after 7 days culture and reached almost its highest level after 10 days culture (Fig. 2C).

It must be mentioned that we used two lines of ASCs prepared differently during primary culture; one was prepared directly without any selection and the other was the cell population from which CD31 positive cells were removed to avoid contamination by intact endothelial cells. After five passages, both lines were examined for vascular endothelial differentiation, no differences between the two groups with respect to the differentiation efficiency were detected.

3.3. Differentiated ASCs express vascular endothelial-specific protein

To examine whether the differentiated ASCs actually expressed vascular endothelial-specific marker proteins, we stained those cells with anti-flk1, anti-tie2, and anti-CD34 antibodies. Most of the cells positively expressed flk1, tie2, and CD34 (Fig. 3A–C). The average of percentages of positive cells calculated by MetaMorph software were as follows: flk1 (82%), tie2 (78%), and CD34 (87%), respectively. These results indicate that approximately 80–90% of the ASCs differentiated into vascular endothelial-like cells.

3.4. VECs differentiated from ASCs showed similar morphological and physiological functions in vitro and in vivo

After ASCs were cultured in DMEM/F12 medium with EGM-2 BulletKit (without FGF2), ITS and 10 ng/ml FGF2 on collagen type IV coated dishes, they were capable of forming tubular-like vascular structures when they were seeded in Matrigel dishes (Fig. 4C). In contrast, ASCs cultured in DMEM containing 5% FBS

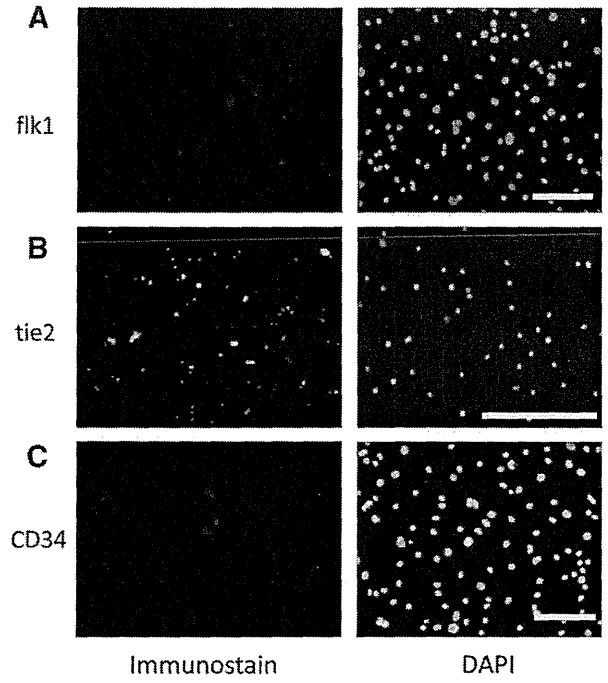

Fig. 3. Immunohistochemical staining of differentiated ASCs with anti-vascular endothelial marker proteins antibodies. All of three marker proteins (flk1, tie2, and CD34) were positively stained against the differentiated ASCs cultured for 12 days in the medium. Calculated with Metamorph software, average of flk1 (A), tie2 (B), and CD34 (C) positive cells were about 82%, 78%, and 87%, respectively ($n = 6$). Nuclei were stained with DAPI. Scale bar, 200 μm.

did not form such structures (Fig. 4A and B). We next examined whether the differentiated cells formed vessel-like structures in vivo. The femoral muscle of a C57BL/6J mouse was injured by liquid nitrogen. Then we injected vascular endothelial-like cells that had differentiated from ASCs derived from GFP mice into the muscle. Two weeks after the injection, we analyzed tissue samples to determine whether the cells histologically contribute to vessel-like structures. We found that GFP positive cells were incorporated into vessel-like structures, indicating that the VECs which were differentiated from ASCs successfully formed these structures (Fig. 4D) but control cells which cultured in DMEM medium containing 5% FBS did not (data not shown). These results suggest that the induced ASCs were able to form tubular structures almost as well as intact endothelial cells in vitro and in vivo.

Finally, we examined the efficiency of differentiation of ASCs into VECs by measuring LDL uptake. Alexa Flour 488-conjugated acetyl-LDL was added to the medium, and fluorescence positive cells were counted by a flow cytometer and observed under a fluorescence microscope. The differentiated ASCs showed very high acetyl-LDL uptake; over 80% of the cells were fluorescence positive (Fig. 4E and F). Undifferentiated ASCs did not uptake acetyl-LDL at all (Fig. 4F).

4. Discussion

In the present study, we showed that mouse ASCs can differentiate into VECs in serum-free medium in vitro. They formed tubular structures in Matrigel culture, and contributed to vessel-like structures in vivo. Analysis of the vascular endothelial function revealed that over 80% of cells incorporated acetyl-LDL during 6 h of culture, indicating most of the cells differentiated into the functional VECs. These results indicate our differentiation method can be useful for the efficient differentiation of VECs from ASCs.

It is well known that early passage ASCs contain VECs. However, these VECs are also reported to disappear when ASCs are continuously cultured until passage 5 [20], indicating that the VECs in adipose tissue do not propagate in the culture medium for ASCs. To rule out the possibility that VECs were contaminating our ASCs, (i) we removed the VECs using anti-CD31 antibody-conjugated beads before the primary culture and (ii) we used ASCs cultured for more than five passages. Both of the cell population almost equally differentiated into VECs; and there was no detectable difference. These results suggest that most of the intact VECs that may exist in a large population of ASCs at first disappear during continuous culture and propagation of ASCs.

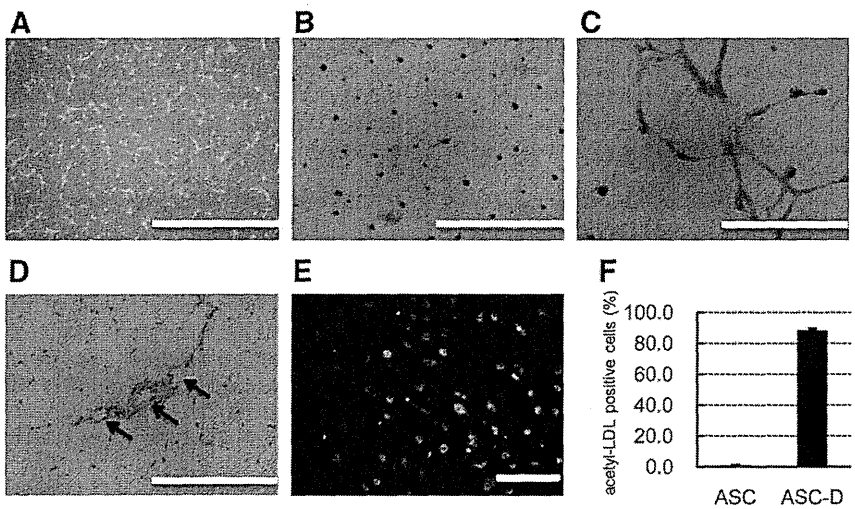

Fig. 4. Morphological and physiological functions of differentiated ASCs. Morphological changes in vascular endothelial-like cells differentiated from ASCs were examined. (A) Normal ASCs were cultured in matrigel for 6 h (A) and 24 h (B). Tubular formation was observed when vascular endothelial-like cells differentiated from ASCs were cultured in matrigel for 24 h (C). Vessel-like structures were formed in the mouse muscle and injected EGFP positive donor cells (brown and arrows) participated in the vessels (D). Acetyl-LDL conjugated fluorescence uptake of differentiated ASCs was examined. Most of the differentiated ASCs were green fluorescence positive when they were cultured in DMEM/F12 medium containing EGM-2 Bulletkit (without FGF2), ITS, and 10 ng/ml FGF2 for 12 days (E). (F) A flow cytometry analysis showed that more than 85% of the differentiated cells (ASC-D) incorporated acetyl-LDL. Normal ASCs did not acetyl-LDL uptake at all (ASC). Scale bar, 2 mm (A–C) and 200 μm (D and E).

FGF2 is a critical growth factor for the induction of VECs. It is reported to play an important role on angiogenesis and vasculogenesis [23–25]. VEGF is also reported to be a key growth factor during embryonic development and differentiation of vascular system [22,26]. We attempted to determine how important and effective these factors are for the induction of VECs in our serum-free condition. We examined the optimal concentrations of these growth factors and demonstrated that the presence of FGF2 upregulated the gene expression of vascular endothelial markers. Therefore, in serum-free conditions, FGF2 is considered an essential growth factor for ASC differentiation into VSC. It is reported that the biologic activity of FGF2 is dependent on the presence of heparin. Small heparin oligosaccharides of defined sizes can activate the mitogenic potential of FGF2 on appropriate target cells and are active in the binding of FGF2 to a soluble FGF2 receptor [27,28]. In the present study, the culture medium contains heparin and it probably upregulates the activity of FGF2. It is possible that heparin plays a critical role in the differentiation from ASCs into VECs in the absence of serum. One the other hand, VEGF did not influence the *tie2* gene expression at any concentration (Fig. 2B) when the culture medium did not contain FGF2. VEGF is reported to be secreted by both mouse [29] and human [30] cultured ASCs, and VEGF expression of VECs is induced by FGF2 [31]. Therefore, additional supplementation with VEGF was not effective for differentiation of VECs in the absence of FGF2 in our experiments.

ASCs were reported to differentiate into VECs when they were cultured in a medium containing FBS [15–18]. FBS contains various unknown factors in varying amounts and may prevent further analysis of the differentiation mechanisms. It is also a negative when cells are prepared for clinical use, because the cells could possibly incorporate proteins or carbohydrates derived from this [32]. The present study intended to establish a medium for differentiation from ASCs to VECs without the usage of FBS. Our method is useful for further analysis of the mechanisms of differentiation from ASCs to VECs and will shed new light on stem cell research.

Acknowledgments

We are grateful to Dr. Barbara Lee Smith Pierce (University of Maryland University College) for editorial work in the preparation of this manuscript. This work was supported by a Grant for National Center for Global Health and Medicine (21A114) and by the grant for Organ Regeneration Project, International Cooperative Research Program, Japan Science and Technology Agency.

Appendix A. Supplementary data

Supplementary data associated with this article can be found, in the online version, at doi:10.1016/j.bbrc.2010.08.029.

References

[1] S. Hombach-Klonisch, S. Panigrahi, I. Rashedi, A. Seifert, E. Alberti, P. Pocar, M. Kurpisz, K. Schulze-Osthoff, A. Mackiewicz, M. Los, Adult stem cells and their trans-differentiation potential—perspectives and therapeutic applications, J. Mol. Med. 86 (2008) 1301–1314.
[2] L. Casteilla, C. Dani, Adipose tissue-derived cells: from physiology to regenerative medicine, Diabetes Metab. 32 (2006) 393–401.
[3] F. D'Andrea, F. De Francesco, G.A. Ferraro, V. Desiderio, V. Tirino, A. De Rosa, G. Papaccio, Large-scale production of human adipose tissue from stem cells: a new tool for regenerative medicine and tissue banking, Tissue Eng. Part C Methods 14 (2008) 233–242.
[4] P.A. Zuk, M. Zhu, P. Ashjian, D.A. De Ugarte, J.I. Huang, H. Mizuno, Z.C. Alfonso, J.K. Fraser, P. Benhaim, M.H. Hedrick, Human adipose tissue is a source of multipotent stem cells, Mol. Biol. Cell 13 (2002) 4279–4295.
[5] P.A. Zuk, M. Zhu, H. Mizuno, J. Huang, J.W. Futrell, A.J. Katz, P. Benhaim, H.P. Lorenz, M.H. Hedrick, Multilineage cells from human adipose tissue: implications for cell-based therapies, Tissue Eng. 7 (2001) 211–228.
[6] G.J. Hausman, Techniques for studying adipocytes, Stain Technol. 56 (1981) 149–154.
[7] G.J. Hausman, D.R. Campion, Histology of the stroma in developing rat subcutaneous adipose tissue, J. Anim. Sci. 55 (1982) 1336–1342.
[8] P. Pettersson, M. Cigolini, L. Sjostrom, U. Smith, P. Bjorntorp, Cells in human adipose tissue developing into adipocytes, Acta Med. Scand. 215 (1984) 447–451.
[9] Y.C. Halvorsen, W.O. Wilkison, J.M. Gimble, Adipose-derived stromal cells—their utility and potential in bone formation, Int. J. Obes. Relat. Metab. Disord. 24 (Suppl. 4) (2000) S41–S44.
[10] Y.D. Halvorsen, D. Franklin, A.L. Bond, D.C. Hitt, C. Auchter, A.L. Boskey, E.P. Paschalis, W.O. Wilkison, J.M. Gimble, Extracellular matrix mineralization and osteoblast gene expression by human adipose tissue-derived stromal cells, Tissue Eng. 7 (2001) 729–741.
[11] M.K. Majumdar, V. Banks, D.P. Peluso, E.A. Morris, Isolation, characterization, and chondrogenic potential of human bone marrow-derived multipotential stromal cells, J. Cell. Physiol. 185 (2000) 98–106.
[12] V. Planat-Benard, J.S. Silvestre, B. Cousin, M. Andre, M. Nibbelink, R. Tamarat, M. Clergue, C. Manneville, C. Saillan-Barreau, M. Duriez, A. Tedgui, B. Levy, L. Penicaud, L. Casteilla, Plasticity of human adipose lineage cells toward endothelial cells: physiological and therapeutic perspectives, Circulation 109 (2004) 656–663.
[13] S. Rangappa, C. Fen, E.H. Lee, A. Bongso, E.K. Sim, Transformation of adult mesenchymal stem cells isolated from the fatty tissue into cardiomyocytes, Ann. Thorac. Surg. 75 (2003) 775–779.
[14] E. Lombardo, O. DelaRosa, P. Mancheno-Corvo, R. Menta, C. Ramirez, D. Buscher, Toll-like receptor-mediated signaling in human adipose-derived stem cells: implications for immunogenicity and immunosuppressive potential, Tissue Eng. Part A 15 (2009) 1579–1589.
[15] H. Nakagami, R. Morishita, K. Maeda, Y. Kikuchi, T. Ogihara, Y. Kaneda, Adipose tissue-derived stromal cells as a novel option for regenerative cell therapy, J. Atheroscler. Thromb. 13 (2006) 77–81.
[16] H. Ning, G. Liu, G. Lin, R. Yang, T.F. Lue, C.S. Lin, Fibroblast growth factor 2 promotes endothelial differentiation of adipose tissue-derived stem cells, J. Sex. Med. 6 (2009) 967–979.
[17] Y. Cao, Z. Sun, L. Liao, Y. Meng, Q. Han, R.C. Zhao, Human adipose tissue-derived stem cells differentiate into endothelial cells in vitro and improve postnatal neovascularization in vivo, Biochem. Biophys. Res. Commun. 332 (2005) 370–379.
[18] J. Oswald, S. Boxberger, B. Jorgensen, S. Feldmann, G. Ehninger, M. Bornhauser, C. Werner, Mesenchymal stem cells can be differentiated into endothelial cells in vitro, Stem Cells 22 (2004) 377–384.
[19] V. Planat-Benard, C. Menard, M. Andre, M. Puceat, A. Perez, J.M. Garcia-Verdugo, L. Penicaud, L. Casteilla, Spontaneous cardiomyocyte differentiation from adipose tissue stroma cells, Circ. Res. 94 (2004) 223–229.
[20] D.O. Traktuev, S. Merfeld-Clauss, J. Li, M. Kolonin, W. Arap, R. Pasqualini, B.H. Johnstone, K.L. March, A population of multipotent CD34-positive adipose stromal cells share pericyte and mesenchymal surface markers, reside in a periendothelial location, and stabilize endothelial networks, Circ. Res. 102 (2008) 77–85.
[21] C. Basilico, D. Moscatelli, The FGF family of growth factors and oncogenes, Adv. Cancer Res. 59 (1992) 115–165.
[22] N. Ferrara, K. Carver-Moore, H. Chen, M. Dowd, L. Lu, K.S. O'Shea, L. Powell-Braxton, K.J. Hillan, M.W. Moore, Heterozygous embryonic lethality induced by targeted inactivation of the VEGF gene, Nature 380 (1996) 439–442.
[23] I. Flamme, W. Risau, Induction of vasculogenesis and hematopoiesis in vitro, Development 116 (1992) 435–439.
[24] J. Folkman, C. Haudenschild, Angiogenesis in vitro, Nature 288 (1980) 551–556.
[25] A. Kurane, N. Vyavahare, In vivo vascular tissue engineering: influence of cytokine and implant location on tissue specific cellular recruitment, J. Tissue Eng. Regen. Med. 3 (2009) 280–289.
[26] P. Carmeliet, V. Ferreira, G. Breier, S. Pollefeyt, L. Kieckens, M. Gertsenstein, M. Fahrig, A. Vandenhoeck, K. Harpal, C. Eberhardt, C. Declercq, J. Pawling, L. Moons, D. Collen, W. Risau, A. Nagy, Abnormal blood vessel development and lethality in embryos lacking a single VEGF allele, Nature 380 (1996) 435–439.
[27] D.M. Ornitz, A. Yayon, J.G. Flanagan, C.M. Svahn, E. Levi, P. Leder, Heparin is required for cell-free binding of basic fibroblast growth factor to a soluble receptor and for mitogenesis in whole cells, Mol. Cell. Biol. 12 (1992) 240–247.
[28] A. Yayon, M. Klagsbrun, J.D. Esko, P. Leder, D.M. Ornitz, Cell surface, heparin-like molecules are required for binding of basic fibroblast growth factor to its high affinity receptor, Cell 64 (1991) 841–848.
[29] S. El-Ftesi, E.I. Chang, M.T. Longaker, G.C. Gurtner, Aging and diabetes impair the neovascular potential of adipose-derived stromal cells, Plast. Reconstr. Surg. 123 (2009) 475–485.
[30] J. Rehman, D. Traktuev, J. Li, S. Merfeld-Clauss, C.J. Temm-Grove, J.E. Bovenkerk, C.L. Pell, B.H. Johnstone, R.V. Considine, K.L. March, Secretion of angiogenic and antiapoptotic factors by human adipose stromal cells, Circulation 109 (2004) 1292–1298.
[31] G. Seghezzi, S. Patel, C.J. Ren, A. Gualandris, G. Pintucci, E.S. Robbins, R.L. Shapiro, A.C. Galloway, D.B. Rifkin, P. Mignatti, Fibroblast growth factor-2 (FGF-2) induces vascular endothelial growth factor (VEGF) expression in the endothelial cells of forming capillaries: an autocrine mechanism contributing to angiogenesis, J. Cell. Biol. 141 (1998) 1659–1673.
[32] M.J. Martin, A. Muotri, F. Gage, A. Varki, Human embryonic stem cells express an immunogenic nonhuman sialic acid, Nat. Med. 11 (2005) 228–232.

CELLULAR REPROGRAMMING
Volume 12, Number 5, 2010

DOI: 10.1089/cell.2009.0104

Epigenetic Differences between Embryonic Stem Cells Generated from Blastocysts Developed *In Vitro* and *In Vivo*

Takuro Horii, Eikichi Yanagisawa, Mika Kimura, Sumiyo Morita, and Izuho Hatada

Abstract

Embryonic stem (ES) cells constitute a very important tool for regenerative medicine today. These ES cells, and human ES cells in particular, are almost all derived from embryos obtained by *in vitro* fertilization (IVF) and from *in vitro* culture (IVC); however, such *in vitro* manipulated embryos often show abnormal genomic imprinting, which can lead to the development of various diseases. Nevertheless, several reports have evaluated ES cells derived from *in vitro* manipulated embryos. In this study, we established ES cells derived from both *in vivo* and *in vitro* developed blastocysts (Vivo ES cells and Vitro ES cells, respectively) to compare the methylation status of imprinted genes and gene expression patterns. At very early passages, Vitro ES cells showed an increase in abnormal genomic imprinting compared to Vivo ES cells. In addition, we found that the gene expression patterns of several methylation related-genes frequently shifted to promote demethylation and to inhibit methylation in early-passage Vitro ES cells. In contrast, at later passages, we found no significant differences between Vivo and Vitro ES cells. In conclusion, it is advisable to use early passage Vivo ES cells whenever feasible, or to select ES cell lines with a normal epigenotype.

Introduction

IN VITRO EMBRYO MANIPULATION TECHNOLOGIES, such as *in vitro* fertilization (IVF), *in vitro* culture (IVC), and other reproduction technologies, have contributed to the development of infertility treatment and animal reproduction. In contrast, a growing number of reports suggest that embryo manipulation *in vitro* increases the risk of diseases such as Angelman Syndrome (AS) and Beckwith-Wiedemann Syndrome (BWS) (Cox et al., 2002; DeBaun et al., 2003; Gicquel et al., 2003; Maher et al., 2003; Orstavik et al., 2003). These diseases are thought to be caused by aberrant genomic imprinting.

Genomic imprinting is the preferential silencing of one parental allele by epigenetic DNA methylation. For example, the expression levels of the *H19* imprinted gene are regulated by an upstream differentially methylated region (DMR) (Bartolomei et al., 1991; Ferguson-Smith et al., 1991; Pfeifer, 2000). The *H19* mRNA is transcribed from the unmethylated maternal allele, but is not transcribed from the methylated paternal allele. In mice, the erasure of genomic imprinting takes place in germ lines between embryonic day (E) 10.5 and E12.5, around the time when primordial germ cells enter the gonads (Szabo and Mann, 1995). Following erasure, DNA methylation patterns are then reestablished in a sex- and sequence-specific manner during gametogenesis. These methylation imprints are then stably maintained during cellular division and differentiation in somatic lineages. The expression levels of imprinted genes are regulated not only by DNA methylation but also by histone modification (Fournier et al., 2002); however, DNA methylation, including genomic imprinting, is regarded as more stable than histone modification in preimplantation embryos (Kim and Ogura, 2009) and brain (Yamasaki et al., 2005).

For the establishment and maintenance of DNA methylation, various enzymes and proteins are indispensable; for example, the cytosine-guanine (CpG) DNA methyltransferases, Dnmt1, Dnmt3a, and Dnmt3b, which coordinately regulate CpG methylation in the genome (Li et al., 1992; Okano et al., 1998, 1999). Dnmt1 is involved in maintenance activity, whereas Dnmt3a and Dnmt3b are mainly responsible for the creation of new methylation patterns. Stella (PGC7), a primordial germ cell and embryonic stem (ES) cell marker, protects against DNA demethylation in early embryogenesis (Nakamura et al., 2007). Zfp57, a putative KRAB zinc-finger protein, is also required for the

Laboratory of Genome Science, Biosignal Genome Resource Center, Institute for Molecular and Cellular Regulation, Gunma University, Gunma, Japan.

postfertilization maintenance of maternal and paternal methylation imprints at multiple imprinted domains (Li et al., 2008). In contrast, the existence of active demethylation factors has rarely been reported in mammals, although the finding that Gadd45 (growth arrest and DNA damage inducible protein 45) interacts with the nucleotide excision repair (NER) complex and promotes DNA demethylation suggests that Gadd45 recruits the DNA repair machinery to specific sites to replace methylated cytosines with unmethylated ones (Barreto et al., 2007; Ma et al., 2009).

The culture conditions of fertilized embryos can also influence the methylation status of genomic imprinting. For example, a suboptimal culture medium can cause aberrant genomic imprinting of the *H19* gene, whereas embryos cultured in potassium simplex optimized medium with added amino acids (KSOMAA) show global gene expression, genomic imprinting, and embryo development resembling that found in *in vivo* developed embryos (Doherty et al., 2000). Long-term culture of ES cells also affects the methylation status of imprinted genes and their totipotency (Dean et al., 1998). It is unclear what causes DNA methylation instabilities of imprinted genes, although some of the factors described above may be related to the instability of imprinted genes.

Mouse ES cells (Evans and Kaufman, 1981; Martin, 1981) can give rise to ectodermal, endodermal, and mesodermal germ layers both *in vivo* and *in vitro*. In human ES cells, several studies have recently provided evidence of the efficient induction of endoderm, mesoderm, and ectoderm, and many of their downstream derivatives (Murry and Keller, 2008), and these reports offer broad perspectives for regenerative medicine. However, all human ES cell lines are established from *in vitro* manipulated embryos that often show abnormal genomic imprinting, which can lead to an increase in the frequency of diseases. Therefore, although it is very important to compare the epigenetic composition of Vivo and Vitro ES cells, there have been few reports characterizing their differences. In this study, we have compared the methylation status of imprinted genes and the gene expression patterns of both Vivo and Vitro ES cell lines in mice, and we have concluded that Vitro ES cells are similar to Vivo ES cells, except at very early passages.

Materials and Methods

Mice

The C57BL/6J mouse strain (B6) was purchased from Charles River Japan. The PWK mouse strain (RBRC00213) was provided by RIKEN BRC (Japan), which is participating in the National Bio-Resource Project of the MEXT, Japan. All animal experiments were conducted according to the guidelines of the Animal Care and Experimentation Committee, Gunma University, Showa Campus, Japan.

Embryo collection and culture

B6 females were superovulated by the injection of five units of pregnant mares' serum (PMSG; ASKA Pharmaceutical, Tokyo, Japan) and 48 h later by five units of human chorionic gonadotrophin (hCG; ASKA Pharmaceutical). For the production of *in vitro* cultured embryos, cumulus–oocyte complexes were collected in TYH medium (Toyoda et al., 1971), from oviducts 16 to 17 h post-hCG injection (p.i.). Spermatozoa were collected from the caudal epididymis of adult PWK, and B6 males and were capacitated by preincubation for 1 h in TYH medium. Cumulus–oocyte complexes were inseminated with capacitated spermatozoa in a humidified atmosphere of 5% CO_2, 95% air at 37°C. Six hours after insemination, the B6xPWK F1 (BPF1) or B6xB6 (B6) fertilized oocytes were washed and cultured in M16 medium supplemented with 0.1 mM EDTA/2Na. The embryos developed into blastocysts at 4.5 days p.i (*in vitro* blastocyst). In contrast, embryos allowed to develop *in vivo* (*in vivo* blastocyst) were collected from females killed at 3.5 days p.i. by flushing their uteri with M2 medium.

Generation of ES cell lines

Both *in vitro* blastocysts at 4.5 days p.i. and *in vivo* blastocysts at 3.5 days p.i. were transferred onto gelatinized tissue culture wells (two to three blastocysts per well of a four-well multiplate) and cultured for 7 days in ES medium, DMEM (Gibco, Gland Island, NY, USA) containing 17.5% Knockout SR (Gibco), following standard procedures (Horii et al., 2008; Robertson, 1987). After 7 days, inner cell mass (ICM) outgrowths were harvested in 0.25% trypsin-EDTA (Gibco), disaggregated by mouth pipetting, and plated onto gelatinized tissue culture wells in ES medium (passage 1). Clones resembling ES cells morphologically were picked and disaggregated a second time. They were then expanded and passaged prior to use.

Alkaline phosphatase (AP) staining

Histochemical staining for AP activity was performed as previously described (Buehr and McLaren, 1993).

Generation of embryoid bodies

For embryoid body (EB) formation, ES cells were detached and dissociated into single cells with trypsin-EDTA and then plated onto a bacteriological dish in 10 mL of DMEM supplemented with 15% fetal bovine serum (Hyclone, Logan, UT, USA), nonessential amino acids (0.1 mM), and 2-mercaptoethanol (0.1 mM).

RNA isolation and reverse transcription

Total RNA was purified from ES cells and EBs using TRIZOL reagent (Invitrogen, Carlsbad, CA), following DNaseI treatment. One microgram of purified RNA was reverse transcribed using Superscript II (Takara Bio, Otsu, Japan) and Oligo(dT)12–18 primer (Takara Bio) in a total volume of 20 μL. For quantitative real-time polymerase chain reaction (PCR), cDNA was diluted 1:10 in distilled water.

Quantitative real-time PCR

Quantitative real-time RT-PCR was performed using SYBR Premix Ex Taq (Perfect Real Time; Takara Bio). The PCR mixture consisted of 2×SYBR Premix Ex Taq, 10 μM forward and reverse primers, 50×ROX reference dye, and 2 μL of template cDNA in a total volume of 12.5 μL. The cocktail was activated by heating initially at 95°C for 10 sec. The subsequent PCR reaction was carried out at 95°C for 5 sec and at 60°C for 30 sec for 40 cycles in an ABI 7700 Sequence Detector. In each run, the dilution series of cDNA

from ES cells or EBs was amplified to serve as a standard curve for the calculation of relative quantities of the target gene using Sequence Detector Software v1.7 (comparative CT method). The *Gapdh* gene was used to standardize the data. All results were obtained from at least two independent experiments and each assay was duplicated. PCR amplification was performed using the primer sets shown in Table 1.

Allele-specific expression analysis

First-strand cDNA was subjected to PCR, which was carried out using LA Taq HS (Takara Bio) and the primer sets shown in Table 1. *H19* gene polymorphisms were detected by RFLP (restriction fragment-length polymorphism). Following RT-PCR, *H19* products were digested with *Bgl* I at 37°C for 3 h and separated on a 2% agarose gel in 0.5×TAE.

DNA isolation and methylation analysis

DNA was isolated from each ES cell line. Bisulfite treatment was carried out using an Epitect Bisulfite kit (Qiagen, Hilden, Germany), according to the manufacturer's instructions. PCR amplification of *H19* DMR, *Snrpn* DMR1, and *Igf2r* DMR2 was performed for each set of isolated cells using the primer set shown in Table 1. The amplification consisted of a total of 35 cycles at 94°C for 10 sec, 55°C (*H19*) or 60°C (*Igf2r* and *Snrpn*) for 30 sec, and 72°C for 60 sec in a GeneAmp PCR system 9700 (Applied Biosystems, Foster City, CA, USA). PCR products were subcloned into the TA cloning vector (pCR 2.1; Invitrogen). Positive clones in each sample were sequenced using the Big Dye terminator method (ABI PRISM 3100; Applied Biosystems). Parental alleles were determined by SNPs (Table 2). Combined bisulfite restriction analysis (COBRA) (Xiong and laird, 1997) of *H19* (annealing 55°C, 35 cycles), *Snrpn* (annealing 60°C, 35 cycles), *Igf2r* (annealing 60°C, 35 cycles), and major satellite (annealing 55°C, 30 cycles) was carried out as previously described (Horii et al., 2008; Morita et al., 2007). Methylation percentages were calculated as previously reported (Xiong and Laird, 1997).

Immunoblot analysis

Whole cell extracts were subjected to 10% SDS-PAGE gel electrophoresis and the protein were transferred to a PVDF membrane. The following antibodies (1:1,000) were used for immunoblotting: anti-Oct3/4 (sc-5279, Santa Cruz, CA, USA), anti-Dnmt3b (kindly donated by Dr. S. Tajima) and anti-α-tubulin (CP06, Calbiochem, Darmstadt, Germany). Signals were detected by chemiluminescence (ECL Plus, GE healthcare, Buckinghamshire, UK) on a CCD camera (LAS-3000, Fujifilm, Tokyo, Japan). Protein band intensities were normalized to those of α-tubulin using Image J software (NIH).

TABLE 1. SEQUENCES OF THE PRIMERS USED FOR RT-PCR

Gene name	*Sequence*	*Product size*	*Gene ID*
Quantitative real-time RT-PCR			
Oct3/4	5′-CCAATCAGCTTGGGCTAGAG-3′ 5′-CTGGGAAAGGTGTCCCTGTA-3′	129 bp	NM_013633
Nanog	5′- ATGCCTGCAGTTTTTCATCC-3′ 5′- GAGGCAGGTCTTCAGAGGAA-3′	109 bp	NM_028016
Stella	5′- AGCCGTACCTGTGGAGAACAA-3′ 5′-TCTTTCAGCACCGACAACAAA-3′	99 bp	NM_139218
Dnmt1	5′-CCTAGTTCCGTGGCTACGAGGAGAA-3′ 5′-TCTCTCTCCTCTGCAGCCGACTCA-3′	137 bp	NM_010066
Dnmt3a	5′-GCCGAATTGTGTCTTGGTGGATGACA-3′ 5′-CCTGGTGGAATGCACTGCAGAAGGA-3′	147 bp	NM_007872
Dnmt3b	5′-TTCAGTGACCAGTCCTCAGACACGAA-3′ 5′-TCAGAAGGCTGGAGACCTCCCTCTT-3′	146 bp	NM_001003961
Zfp57	5′-TATGAGGACGTGGCAGTGTC-3′ 5′-GGAGGACTTCTCCTGCTCCT-3′	186 bp	NM_009559
Gadd45a	5′-TGCACTGTGTGCTGGTGAC-3′ 5′-CGGCAAAAACAAATAAGTTGA-3′	79 bp	NM_007836
Gadd45b	5′-GAGACCTGCACTGCCTCCT-3′ 5′-TTGCCTCTGCTCTCTTCACA-3′	100 bp	NM_008655
Cdx2	5′-TCCCTAGGAAGCCAAGTGAA-3′ 5′-CTGCGGTTCTGAAACCAAAT-3′	188 bp	NM_007673
Gata6	5′-GCCAACTGTCACACCACAAC-3′ 5′-GTTACCGGAGCAAGCTTTTG-3′	189 bp	NM_010258
T	5′-GCTCCCCTGCACATTACACA-3′ 5′-TGACTGTAGCAGCCCCTTCA-3′	96 bp	NM_009309
Nestin	5′-CTGCAGGCCACTGAAAAGTT-3′ 5′-AGGTGTCTGCAAGCGAGAGT-3′	189 bp	NM_016701
Gapdh	5′-AATGCATCCTGCACCACCAA-3′ 5′-GTGGCAGTGATGGCATGGAC-3′	106 bp	NM_008084
Allelic expression			
H19	5′-CGGAGATAGCTTTGAGTCTC-3′ 5′-ATTGATGGACCAGGACCTCT-3′	248 bp	NR_001592

TABLE 2. SEQUENCES OF THE PRIMERS USED FOR BISULFITE SEQUENCING

Gene name	*Sequence*	*Size*	*Gene ID*	*SNPs*
*H19*DMR	5′-GGATATATGTATTTTTTAGGTTGGT-3′ 5′-AAAAAAACTCAATCAATTACAATCC-3′	174 bp	MMU19619	58 G(B6)/A(PWK), 128 T(B6)/G(PWK), 146 A(B6)/G(PWK)
Snrpn DMR1	5′-TTTGGTAGTTGTTTTTTGGTAGGATAT-3′ 5′-ACTAAAATCCACAAACCCAACTAAC-3′	248 bp	AF081460	36 G(B6)/A(PWK), 44 G(B6)/T(PWK)
Igf2r DMR2	5′-GAAGGGTTTTGTGATTAGGGTTAA-3′ 5′-AACACCTTCATATACCCCTAAACAC-3′	286 bp	L06446	51 A(B6)/G(PWK) (Kobayashi et al., 2006)

Statistical analysis

Data are shown as means and standard deviations. The Student's *t*-test was used for methylation, gene expression, and immunoblot analyses, and a *p*-value of <0.05 was considered significant. The statistical analyses were performed with Excel X and Statcel2 for Macintosh. QUMA (QUantification tool for Methylation Analysis; http://quma.cdb.riken.jp/) was used for statistical analyses of the bisulfite sequencing of CpG methylation (Kumaki et al., 2008).

Results

Establishment of ES cell lines

Freshly collected *in vivo* blastocysts and *in vitro* cultured blastocysts were prepared for the establishment of ES cell lines. The embryos obtained *in vivo* had developed to the blastocyst stage at the time they were flushed (3.5 days p.i.), whereas 1 extra day in culture (4.5 days p.i.) was necessary to obtain *in vitro* cultured blastocysts (Fig. 1A). Both *in vivo* and *in vitro*-derived blastocysts were used for establishing ES cell lines. All ES cell lines obtained formed densely packed colonies and showed AP activity (Fig. 1B). The efficiency of ES cell establishment was not significantly different between *in vivo* and *in vitro* developed blastocysts (Table 3).

Methylation status and gene expression at early passages

The imprinting of the *H19* gene, one of the paternally methylated genes, is stably maintained during cellular division and differentiation, and is transcribed exclusively from the maternal allele. It was also thought that the imprint was maintained during preimplantation development (Pfeifer, 2000). In contrast, some researchers have demonstrated that normal imprinting can be disrupted during preimplantation development, resulting in biallelic expression of the *H19* gene (Doherty, et al., 2000; Mann, et al., 2004; Sasaki, et al., 1995). To investigate whether Vitro ES cells take on abnormal imprinting from *in vitro* cultured blastocysts, we performed methylation

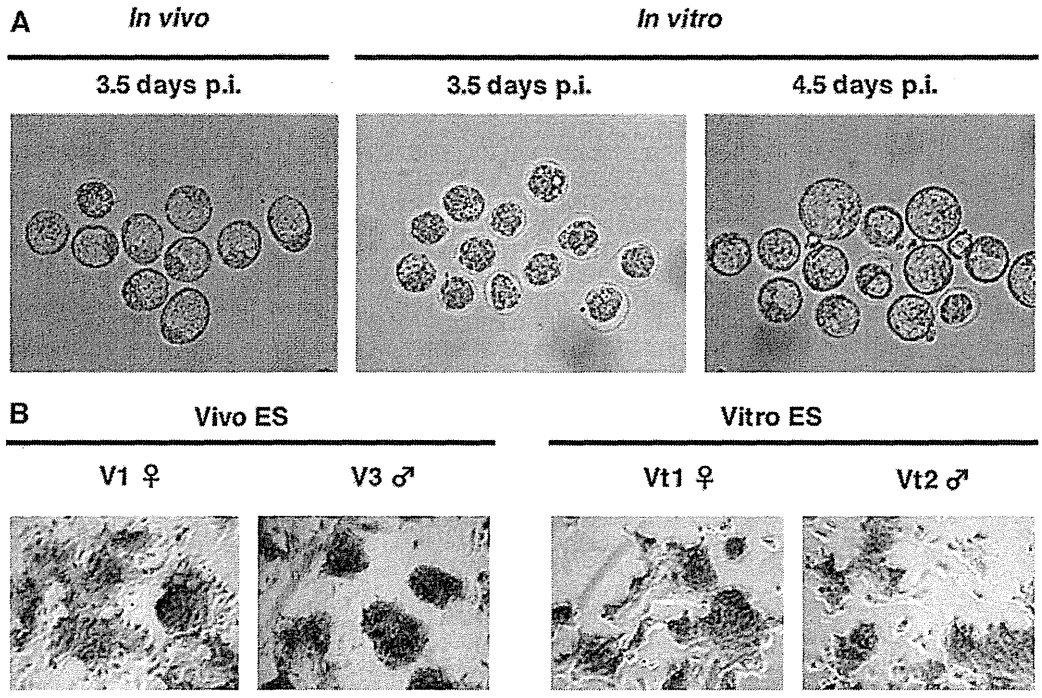

FIG. 1. Establishment of Vivo and Vitro ES cells (BPF1 mouse strain). (**A**) Representative morphology of blastocysts developed *in vivo* and blastocysts cultured *in vitro*. (**B**) Both Vivo and Vitro ES cells show alkaline phosphatase (AP) activity.

TABLE 3. EFFICIENCY OF ES CELL ESTABLISHMENT FROM BPF1 AND B6 BLASTOCYSTS

Mouse strain	*Origin of blastocyst*	*Total number of explants*	*Number giving ES cell lines (%)*
BPF1	*In vivo*	10	8 (80)
BPF1	*In vitro*	28	20 (71)
B6	*In vivo*	18	9 (50)
B6	*In vitro*	15	8 (53)

analysis of the *H19* DMR for early passage cells (passage 2). The results of bisulfite sequencing showed that the *H19* DMR on the paternal allele was more widely demethylated in Vitro ES cells than in Vivo ES cells (Fig. 2), as was reported for *in vitro* cultured blastocysts (Doherty et al., 2000). Other imprinted genes, *Snrpn* DMR1, and *Igf2r* DMR2, did not show large differences (Fig. 3), although the average methylation levels of Vivo ES cells were higher than those of Vitro ES cells. COBRA analysis confirmed that the *H19* DMR was significantly demethylated in Vitro ES cells compared to Vivo ES cells at the *Hinf* I site (Fig. 4). *Igf2r* DMR2 also showed significant differences in COBRA (Fig. 4), but not in bisulfite sequencing. On the basis of the bisulfite sequencing and COBRA results, the methylation status of *H19* DMR was judged more unstable than that of other imprinted genes and satellite repeats.

Next, we assessed gene expression patterns in ES cells at early passages by quantitative real-time RT-PCR. The expression of *Oct3/4* mRNA, a pluripotent cell marker, was significantly higher in early passage Vivo ES cells than in Vitro ES cells; whereas other pluripotent marker genes showed no significant differences in expression levels between the two types of ES cells (Fig. 5A). Among the methylation-related genes, mRNA expression of the *de novo* DNA methyltransferase, *Dnmt3b*, was significantly higher in Vivo ES cells (Fig. 5B). *Gadd45b* mRNA expression, which is considered to be one of the putative demethylation factors, was higher in Vitro ES cells (Fig. 5B). On the other hand, there was no difference in *Zfp57* and *Stella* mRNA expression, which is essential for the maintenance of genomic imprinting (Fig. 5A and B), although *Zfp57* expression was significantly different in B6 ES cell lines (Supplemental Fig. 1; see online supplementary

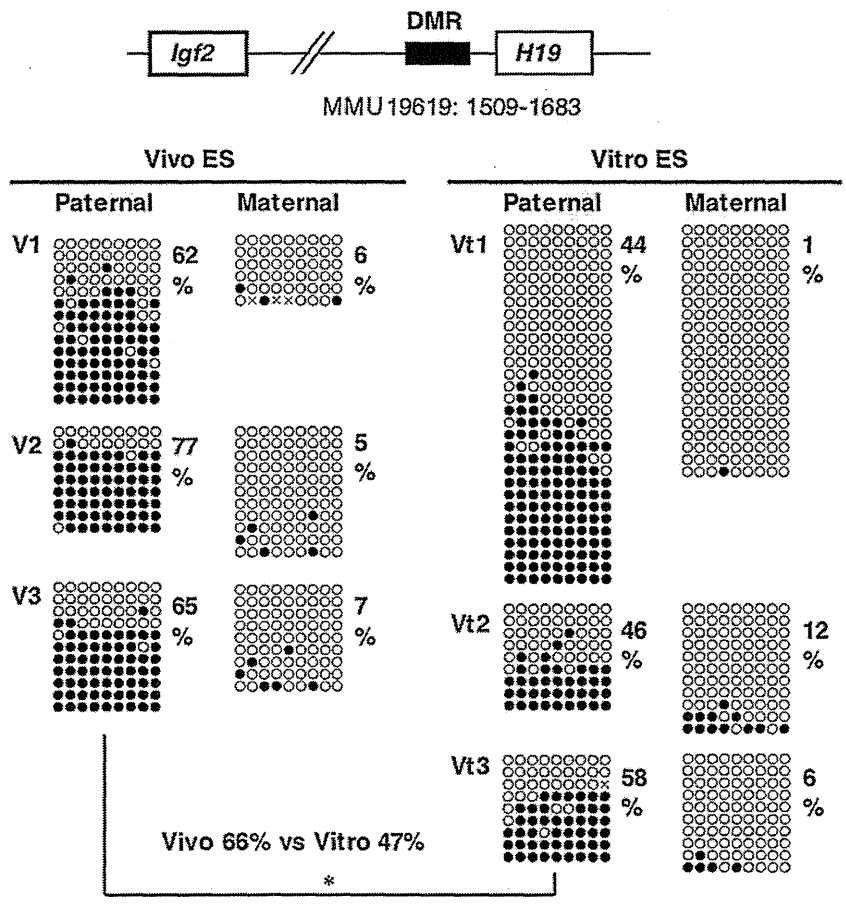

FIG. 2. Methylation status of the *H19* DMR at early passages (passage two) in Vivo and Vitro ES cells (BPF1 mouse strain). Bisulfite sequencing analysis of paternal and maternal alleles was carried out for Vivo and Vitro ES cells. The PCR product was subcloned, and clones were subjected to nucleotide sequencing analysis. The methylation status, either unmethylated (open circle) or methylated (closed circle), is indicated at each CpG site. Percentages of methylated CpGs are shown to the right of the sequences. Vitro ES cells show significantly greater demethylation than Vivo ES cells on the paternal allele of the *H19* DMR ($*p < 0.05$).

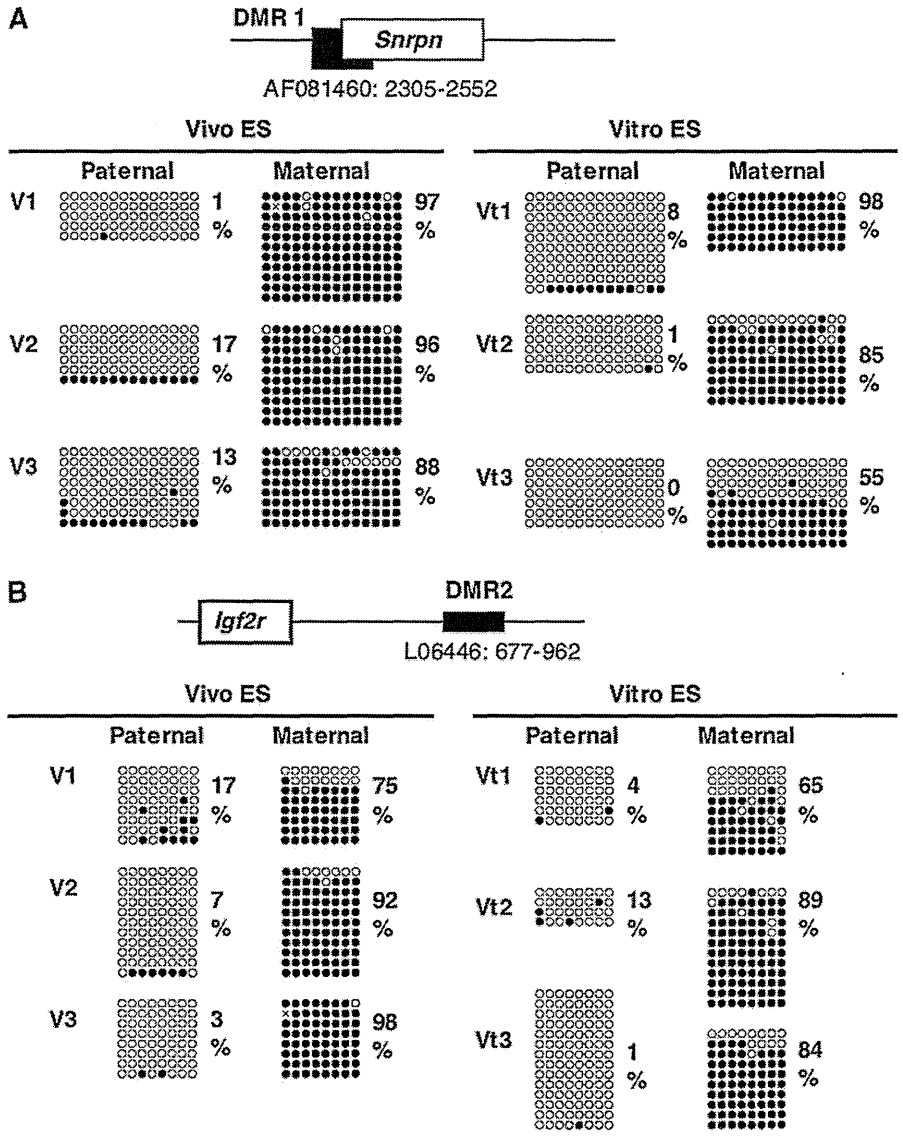

FIG. 3. Methylation status of the *Snrpn* DMR1 and *Igf2r* DMR2 at early passages (passage 2) in Vivo and Vitro ES cells (BPF1 mouse strain). Bisulfite sequencing analysis of paternal and maternal alleles was carried out for Vivo and Vitro ES cells. The PCR product was subcloned, and clones were subjected to nucleotide sequencing analysis. The methylation status, either unmethylated (open circle) or methylated (closed circle), is indicated at each CpG site. Percentages of methylated CpGs are shown to the right of the sequences.

material at www.liebertonline.com). Thus, mRNA expression patterns of several methylation related-genes tend to shift, resulting in the promotion of demethylation and the inhibition of methylation in Vitro ES cells. Nevertheless, there were no significant differences in Oct3/4 and Dnmt3b expression as judged by immunoblot analysis (Fig. 5C).

Methylation status and gene expression at later passages

Both Vivo and Vitro ES cells were passaged several more times, and the methylation status of the *H19* DMR was investigated at later passages. Results from COBRA analysis and bisulfite sequencing at passage five showed no significant differences between Vivo and Vitro ES cells (Figs. 6 and 7). Even Vivo ES cells exhibited highly demethylated alleles (V4 and V6 lines); in contrast, some Vitro ES cells had an almost normally methylated allele (Vt2 line). There was no difference between Vivo and Vitro ES cells in the methylation status of other genes (Fig. 7). This indicates that the methylation status of ES cells at later passages depends more on the character of individual cell lines than on the origin of the ES cells. We then assessed mRNA expression (Fig. 8A and B) and protein expression (Fig. 8C) by real-time RT-PCR and

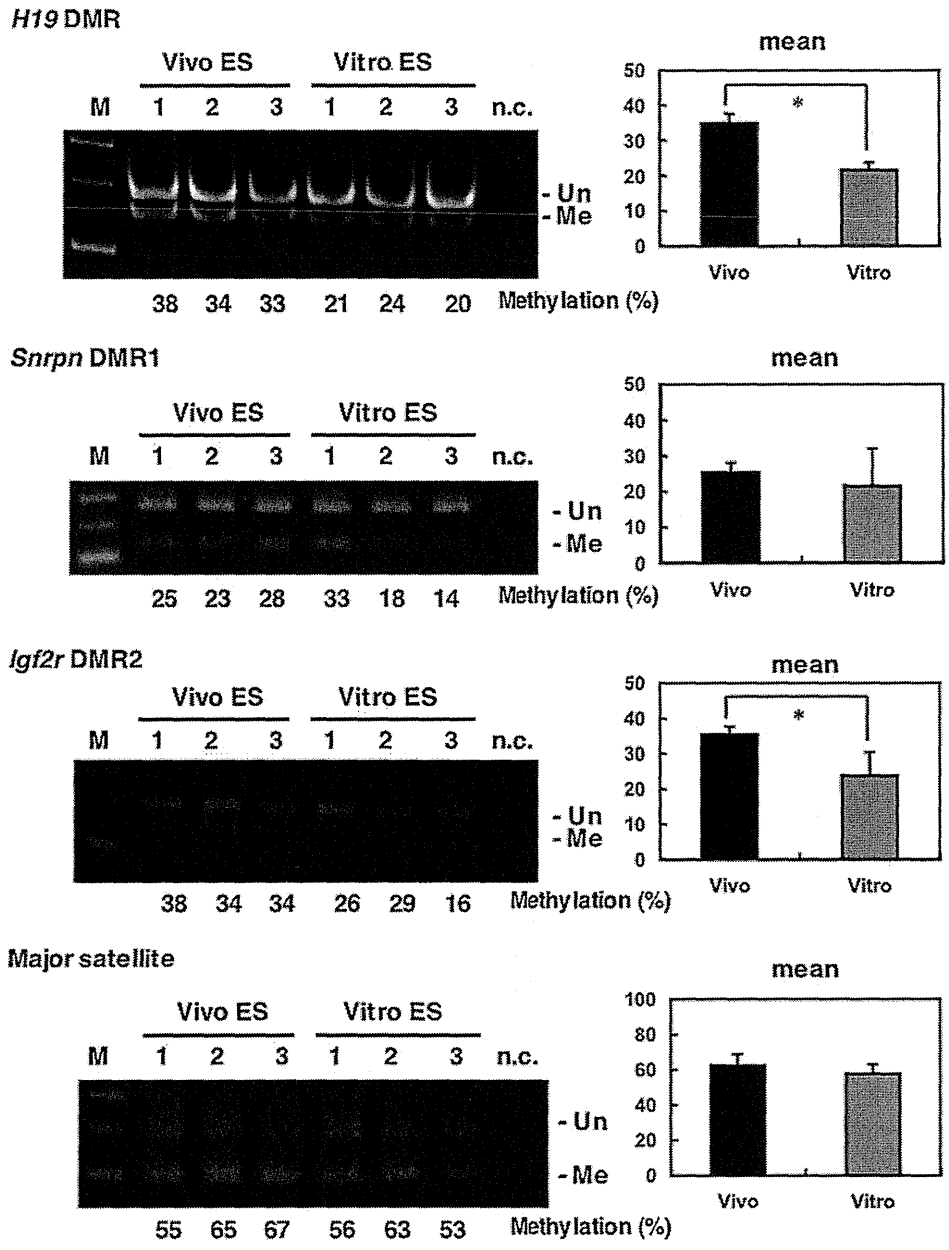

FIG. 4. Methylation status of imprinted genes and satellite repeats at early passages (passage 2) in Vivo and Vitro ES cells (BPF1 mouse strain). COBRA analysis shows that Vitro ES cells are significantly demethylated in *H19* and *Igf2r* DMRs (*$p < 0.05$). M: marker, n.c: negative control, Un: unmethylated, Me: methylated.

immunoblot analyses, respectively, at later passages and, as expected, we found no significant differences between Vivo and Vitro ES cells with respect to pluripotent marker genes and methylation-related genes.

Gene expression after differentiation induction

The differentiation of ES cells in suspension into EBs mimics, at a rudimentary level, events occurring at the late pre- and early postimplantation stages (Doetschman et al., 1985; Martin, 1975; Stevens, 1975). We investigated the allelic expression of the *H19* imprinted gene using EBs obtained at day 5 postsuspension culture. Although it is known that *H19* RNA is transcribed from the unmethylated maternal allele, biallelic expression of *H19* was frequently observed by PCR-RFLP analysis, regardless of the origin of the ES cells (Fig. 9A), indicating that normal genomic imprinting is disrupted in both Vivo and Vitro ES cell lines at later passages. Another imprinted gene, *Snrpn*, also exhibited biallelic expression at later passages (data not shown). To compare the pluripotency of Vivo and Vitro ES cells, we assessed mRNA expression, specific to the three germ layers, by real-time RT-PCR. No

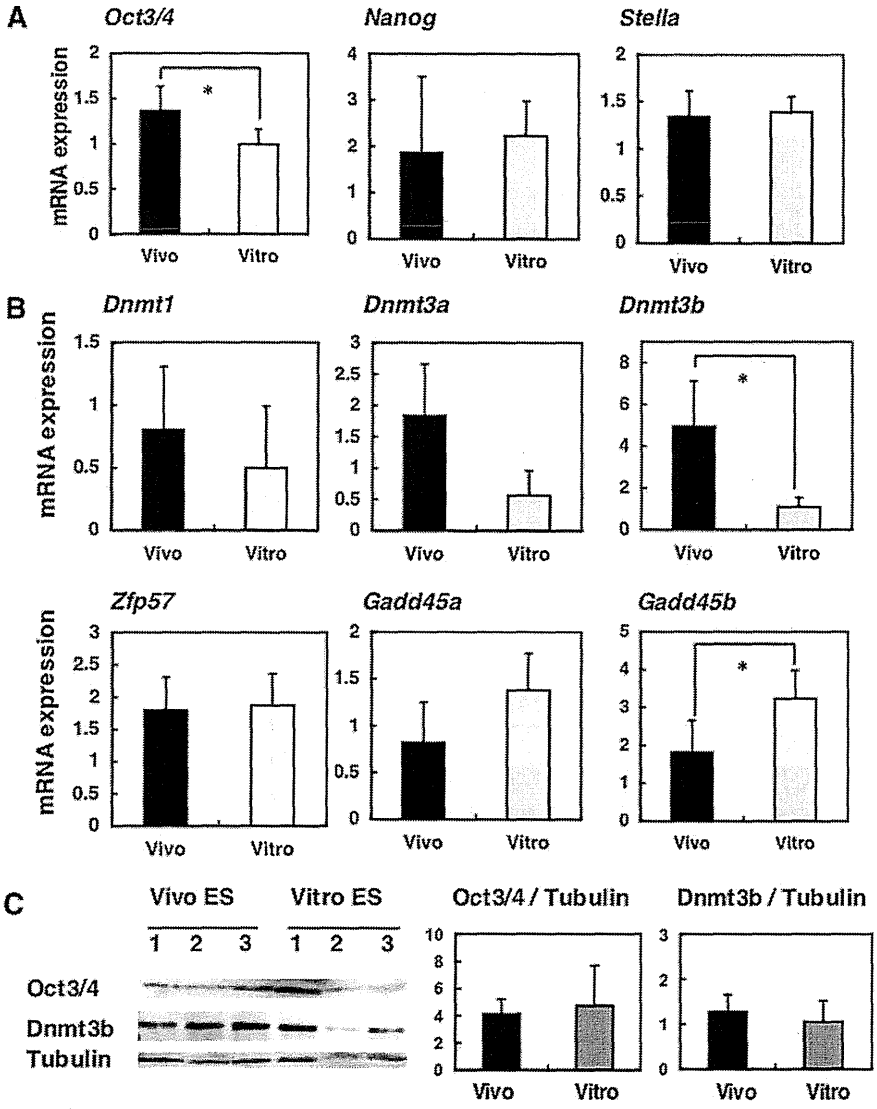

FIG. 5. Expression patterns of early passage (passage 2) Vivo and Vitro ES cells (BPF1 mouse strain). (**A**) Quantitative real-time PCR analysis for ES cell markers (*Oct3/4*, *Nanog*, and *Stella*). (**B**) Quantitative real-time PCR analysis for three DNA methyltransferases (*Dnmt1*, *Dnmt3a*, and *Dnmt3b*), and three putative methylation-related genes (*Zfp57* and *Gadd45*). Data are the means ± standard deviations ($n = 6$): $^*p < 0.05$. (**C**) Immunoblot analysis with anti-Oct3/4 and anti-Dnmt3b. Anti-α-tubulin was to normalize the data. Data are the means ± standard deviations.

significant differences were found for *Cdx2* (trophectoderm), *T* (mesoderm), *Gata6* (primitive endoderm), and *Nestin* (neural progenitor) (Fig. 9B). This result indicates that Vitro ES cells have the same differentiation capabilities as Vivo ES cells in an *in vitro* environment.

Discussion

Several studies have investigated the development of blastocysts *in vitro*; however, little is known about ES cell lines generated from these blastocysts. In humans, the collection of blastocysts *in vivo* is not an option due to ethical issues; thus, the only alternative is to obtain blastocysts through the techniques of IVF, IVC, and other reproduction technologies. In this study, we have compared the methylation status of imprinted genes and gene expression patterns in mouse ES cell lines derived from freshly collected *in vivo* blastocysts and from blastocysts cultured *in vitro*.

The expression of *Oct3/4* in ES cells is essential for the maintenance of pluripotency. The loss of *Oct3/4* expression has been correlated with a progressive loss of pluripotency upon spontaneous differentiation. The level of *Oct3/4* mRNA is significantly higher in freshly collected *in vivo* blastocysts compared to blastocysts cultured *in vitro* (Tielens et al., 2006). Higher levels of *Oct3/4* expression in blastocysts developed *in vivo* leads to a higher efficiency of ES cell line establishment when compared to the establishment of ES cell lines from blastocysts cultured *in vitro* (Tielens et al., 2006).

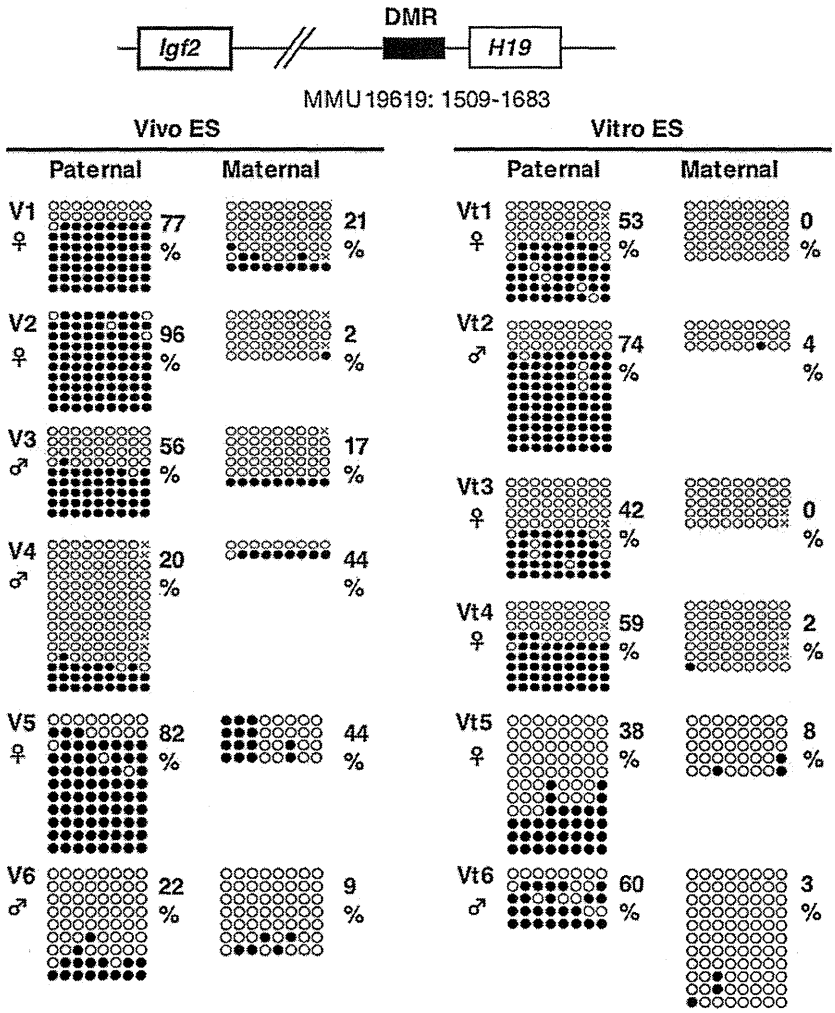

FIG. 6. Methylation status of the *H19* DMR at later passages (passage 5) of Vivo and Vitro ES cells (BPF1). Bisulfite sequencing analysis for both paternal and maternal alleles was carried out for both Vivo and Vitro ES cells. The methylation status, either unmethylated (open circle) or methylated (closed circle), is indicated at each CpG site. Percentages of methylated CpGs are shown to the right of the sequences. There was no significant difference between the ES cell lines.

However, in our study, we found no significant differences in establishment efficiency between Vivo and Vitro ES cells.

One of the reasons for similar establishment efficiencies may be that we used chemically defined knockout serum replacement (Knockout SR) for the establishment of ES cells in this study. In general, fetal bovine serum (FBS) is used as a component of the culture medium for ES cell establishment; however, FBS contains undefined factors, which occasionally stimulate the differentiation of ES cells (Horii et al., 2003). Therefore, the establishment of ES cell lines from blastocysts cultured *in vitro* is difficult if using FBS supplemented medium, because blastocysts with low levels of *Oct3/4* mRNA expression are more easily differentiated by undefined factors (Tielens et al., 2006). In contrast, Knockout SR does not appear to contain these factors, and even if expression levels of *Oct3/4* are low, ES cells can be generated from *in vitro* blastocysts as well as *in vivo* blastocysts, leading to a higher efficiency of establishment for Vitro ES cells than with FBS-supplemented medium. Despite the high establishment efficiency of the Vitro ES cells, the mRNA expression levels of the *Oct3/4* gene were still lower in early passage (passage 2) Vitro ES cells than in Vivo ES cells, although the protein expression levels were the same as judged by immunoblot analysis. The difference between mRNA and protein expression data could be explained by the small difference in the mRNA expression data, which would have been difficult to detect by immunoblot analysis. In contrast, at later passages (passage 5 or 6), no significant differences in the expression levels of ES cell marker genes between in Vivo and Vitro ES cells were detected. We consider that ES cells with higher expression levels of ES cell marker genes might be able to survive more passages than ES cells with lower expression of these genes.

Next, we focused on genomic imprinting in ES cells. In general, imprinted genes are stably maintained during cellular division and differentiation (Pfeifer, 2000). In contrast,

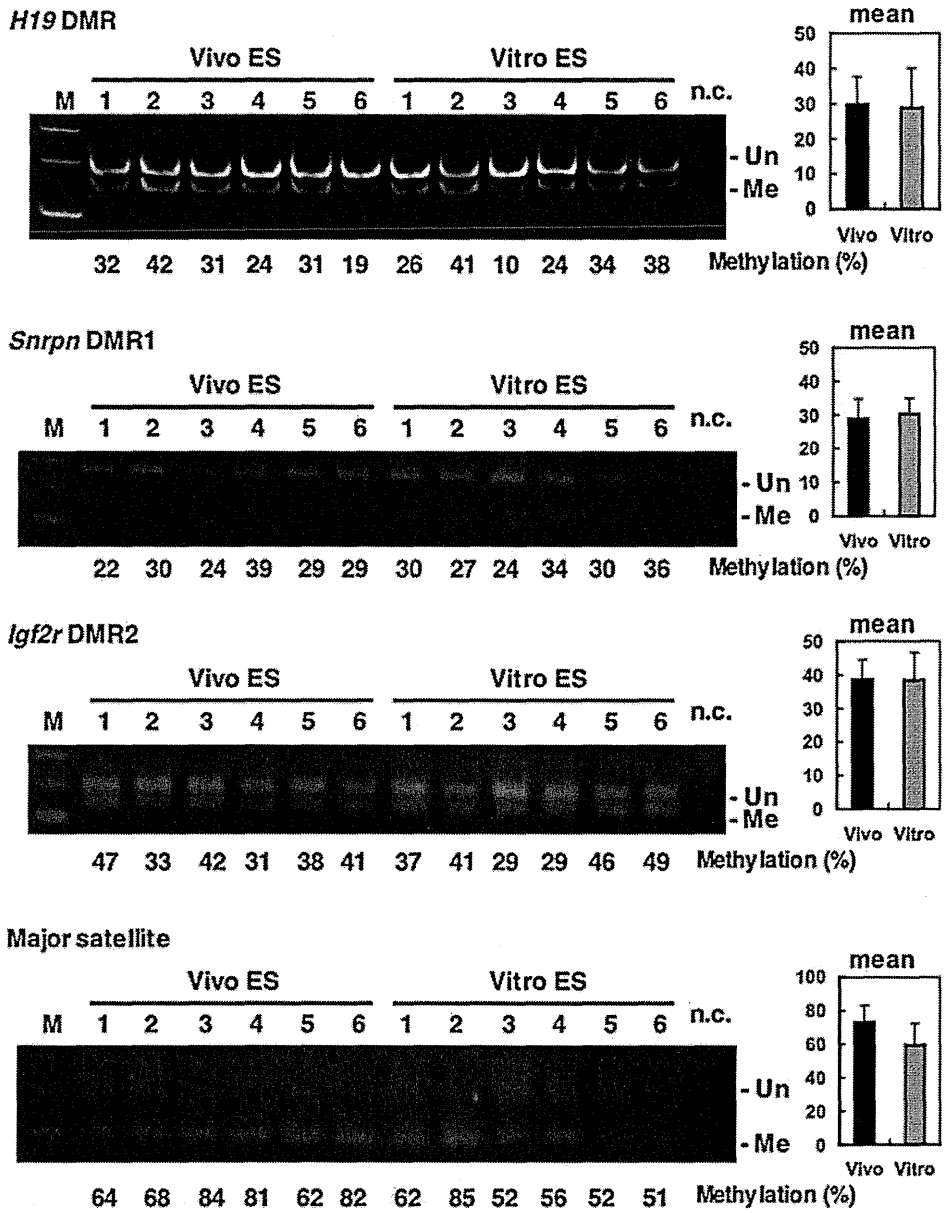

FIG. 7. Methylation status of imprinted genes and satellite repeats at later passages (passage 5) in Vivo and Vitro ES cells (BPF1 mouse strain). There was no significant difference in the percentage of methylated sites for either ES cell line. M: marker, n.c: negative control, Un: unmethylated, Me: methylated.

normal imprinting can be easily disrupted during preimplantation development *in vitro*. For example, *in vitro* cultured blastocysts often exhibit hypomethylation of the *H19* DMR, which results in the biallelic expression of the *H19* gene (Doherty et al., 2000; Mann et al., 2004; Sasaki et al., 1995). In our study, abnormal imprinting was still observed in early-passage Vitro ES cells. According to the expression analysis at this time point, *Dnmt3b* mRNA expression levels were significantly lower in Vitro ES cells than in Vivo ES cells. Dnmt3b is well known as a *de novo* methyltransferase, and is required for the establishment of new methylation patterns during embryonic development (Okano et al., 1999). Dnmt3b is also required for the maintenance of DNA methylation in addition to the major maintenance methyltransferase Dnmt1 (Dodge et al., 2005). These reports suggest that low expression levels of Dnmt3b may result in unstable genomic imprinting in Vitro ES cells.

In addition, hypomethylation in XX ES cells is associated with reduced levels of Dnmt3a and Dnmt3b, and it is known that the ectopic expression of these factors restores global methylation levels (Zvetkova et al., 2005), which supports our hypothesis. However, the demethylation of the *H19*